MAIN-SEQUENCE STARS WITH CIRCUMSTELLAR SOLID MATERIAL: THE VEGA PHENOMENON

DANA E. BACKMAN
NASA Ames Research Center

and

FRANCESCO PARESCE
Space Telescope Science Institute

Solid grains with temperatures of 50 to 125 K and fractional bolometric luminosities ($L_{grains}/L_{\star}$) in the range 10^{-5} to 10^{-3} were found early in the IRAS mission around three nearby A main-sequence stars, α Lyrae (Vega), α Piscis Austrinus (Fomalhaut), and β Pictoris. Spatial resolution of the emission indicates that: (1) the grains are larger than interstellar grains; (2) the material probably lies in disks in the stellar equatorial planes; (3) the disks extend to distances of 100 to 1000 AU from the stars; and (4) zones a few tens of AU in radius around the central stars are relatively empty. The total mass included in the small grains in each case is only 10^{-3} to 10^{-2} $M_{\oplus}$ although more mass could be in undetectable larger bodies. Subsequent surveys of IRAS data reveal more than 100 main-sequence stars of all spectral classes having unresolved excesses with similar temperatures and fractional luminosities to the three prototypes. Some stars with excesses have estimated ages of 1 to 5 Gyr. Thus, main-sequence far-infrared excesses appear to be widespread and are present in systems old enough to be probably past the stage of active planet formation. The sizes of these disks correspond most closely to the hypothetical Kuiper disk reservoir of short-period comets that is supposed to lie in the ecliptic plane just outside the planetary region of our solar system.

I. INTRODUCTION

Expecting to obtain routine calibration observations of α Lyrae during the first months of 1983, IRAS science team members instead found a powerful source of far-infrared radiation an order of magnitude brighter than the emission from the star's photosphere at wavelengths of 60 and 100 μm. Turning to other stars, they discovered several more with similarly strong excesses. Initial studies of the infrared sources around α Lyrae (Vega) (Aumann et al. 1984), α Piscis Austrinus (Fomalhaut), and β Pictoris (Gillett 1986) resulted in the exciting realization that these objects were the first main-sequence stars apart from our Sun known to have attendant solid material in the absence of significant mass loss. Those studies made it clear that the emission was

caused by thermal radiation from grains warmed by the respective stars to temperatures of about 50 to 125 K.

As a result of the IRAS announcements Smith and Terrile (1984) observed β Pic with a coronagraph also constructed for investigations of planetary rings and satellites (Vilas and Smith 1987). Their images revealed that the grains lie in an edge-on disk, considered strong evidence of a relationship between this object and a planetary system. It was initially thought that the material detected by IRAS might represent ongoing planet formation because these three stars are in spectral class A and have lifetimes of order 10^9 years or less, roughly corresponding to the era of planet formation and subsequent heavy bombardment in our solar system. However, investigators continuing to survey the IRAS data have found more than 100 additional examples of similar far-infrared excesses around main-sequence stars of all types and ages.

This review will cover relevant physics and astronomy background information in Sec. II, observations and models of the three spatially resolved examples in Sec. III, search methods and general properties revealed by surveys in Sec. IV, time scales and evolution in Sec. V, and plausibility of a connection between these objects and our solar system in Sec. VI. The latter section includes a comparison between the characteristics of the Vega phenomenon and possible properties of the Kuiper disk.

Several notes of caution are necessary:

1. Almost all the information about these systems comes from IRAS, supplemented in a few cases by groundbased infrared and sub-millimeter observations and in only one case (β Pic) by visual wavelength images. Thus, the available data are limited.
2. It is not clear whether the sources of far-infrared excess in the 100+ candidate systems are the same as in the three resolved prototypes despite similar excess color temperatures and fractional luminosities ($L_e/L_\star$). Until the candidates are resolved by present or future telescopes such as HST, ISO, SOFIA, or SIRTF, the physical mechanism remains uncertain. However, for the purposes of this review these numerous candidates will be considered as examples of the Vega phenomenon.
3. The properties of the three resolved examples which suggest planetary systems are inferred with varying degrees of certainty but are not directly observed. Those properties are: (a) grains larger than interstellar grains; (b) material orbiting rather than falling into or flowing away from the stars; (c) material arranged in disks in the stellar equatorial planes rather than, e.g., in spherical clouds; (d) central regions similar in size to the planetary region of our solar system which are relatively lacking in small grains; (e) a necessary reservoir of larger undetected parent bodies to resupply the presently observed small grain population against various rapid removal processes; (f) transient spectral absorption line events attributed to comets impacting β Pic. These inferences will be examined in later sections.

II. INFRARED EMISSION FROM STARS AND GRAINS

A. Expectations for Stellar Photospheres in the Infrared

The peak emission of even the coolest stars, $T_{\rm eff}\sim$2500 K, occurs at wavelengths shorter than 2.5 μm. The continuum flux densities of stars follow a Rayleigh-Jeans (RJ) slope ($F_\nu \propto \lambda^{-2}$) to about 10% accuracy from wavelengths of 3 to 30 μm and greater, with real stellar infrared continua generally being slightly steeper than RJ (see, e.g., Dreiling and Bell 1980; Engelke 1990 and references therein). Thus, it is relatively easy to estimate the far-infrared flux from a star given its flux at shorter wavelengths and to distinguish excess flux which is not photospheric. An excess with a given luminosity which itself has a spectrum like a Planck function will be more easily detected the cooler it is with respect to the star.

Determination of far-infrared photospheric and excess flux requires a choice of wavelengths at which a star's photosphere can be confidently considered the sole source of significant flux. Figures 1 and 2 compare the observed spectral energy distributions of four systems having strong far-infrared excesses with those of four stars which have little or no far-infrared excess but similar spectral types and similar near-infrared (1–5 μm) colors (see, e.g., Johnson 1966; Koornneef 1983*a*, *b*).

B. Thermal Emission from Grains

Temperatures of spherical grains warmed by stellar radiation can be calculated from equilibrium between absorbed and emitted energy:

$$g_1 \pi a^2 \left(\frac{R_\star}{r}\right)^2 \int_0^\infty \pi \epsilon_\nu B_\nu(T_\star) {\rm d}\nu = 4 g_2 \pi a^2 \int_0^\infty \pi \epsilon_\nu B_\nu(T_g) {\rm d}\nu \qquad (1)$$

where a is the grain radius, r is the distance of the grain from the illuminating star, g_1 and g_2 are geometric factors depending on grain shape, conductivity, and rotation, and ϵ is the grain radiative efficiency. The spectrum of the star is assumed to be a Planck distribution with $T_\star$ equal to the effective temperature $T_{\rm eff}$. If a grain is small or thermally conductive or rapidly rotating such that its entire surface is at the temperature T_g, then $g_1 = g_2$.

The efficiency parameter ϵ is crucial to consideration of the thermal equilibrium of solid material. Particles efficiently absorb and emit radiation with wavelengths smaller than the grain size, but not with wavelengths much larger than the grain size. For a given grain size a and ignoring spectral features of the grain material, ϵ can be considered roughly constant, $\epsilon\sim$(1-albedo)$\sim$1, for absorption and emission of radiation of wavelengths shorter than a critical wavelength $\lambda_o \sim a$. Efficiency ϵ decreases for interaction with radiation of wavelength longer than λ_o.

The ratio between critical wavelength λ_o and grain radius, $\xi \equiv \lambda_o/a$, can vary widely depending on the grain optical properties. For example, $\xi\sim 2\pi$ for strongly absorbing material, while $\xi\sim 1/2\pi$ for weakly absorbing

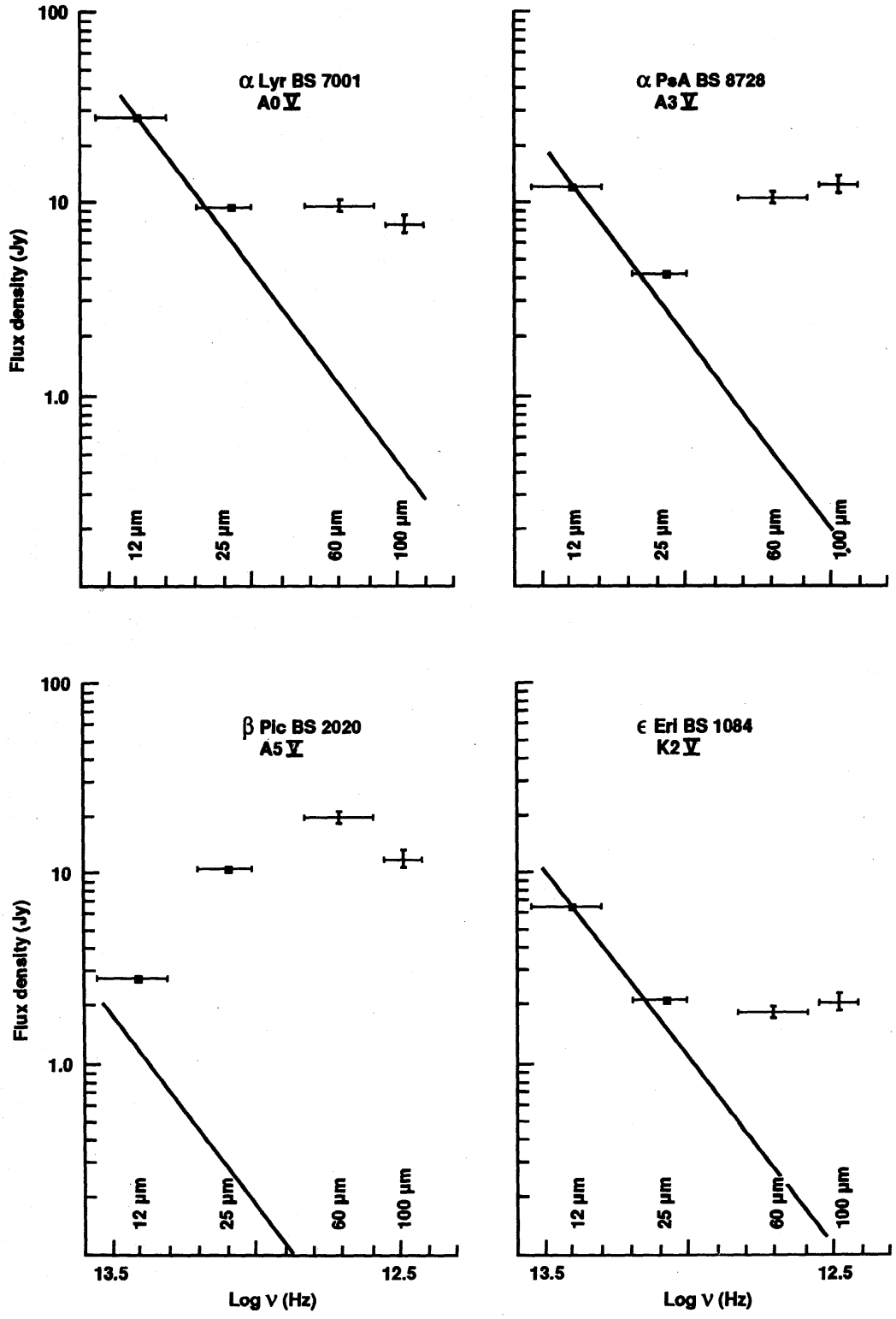

Figure 1. Spectral energy distribution of four nearby main-sequence stars with strong far-infrared excesses detected by IRAS. The diagonal lines show Rayleigh-Jeans extrapolations of the 3.5 μm (L-band) photospheric flux densities. The four excesses have 25–100 μm color temperatures which imply flux densities at 3.5 μm of less than 10^{-10} of the photosphere. The flux density uncertainties include uncertainties in the absolute calibration (figure courtesy of F. C. Gillett 1986).

material. A value of $\xi \sim 1$ may correspond roughly to moderately absorbing dielectrics like "dirty ice" (see, e.g., Greenberg 1978).

The decrease in radiative efficiency for $\lambda > \lambda_o$ can be described by a power law in λ with exponent controlled by the grain properties. A slope $\epsilon \sim (\lambda_o/\lambda)^1$ is appropriate for amorphous materials whereas a steeper decrease $\epsilon \sim (\lambda_o/\lambda)^2$ corresponds to crystalline dielectrics and metals (see, e.g., review by Witt 1989). Grains in the interstellar medium (ISM) may be characterized by an exponent value of about 1.5 (see, e.g., review by Helou 1989).

Assumption of power law absorptive and emissive efficiencies allows an analytic solution to Eq. (1). Specifically, if, ϵ (absorp) is $\epsilon_o(\lambda_o/\lambda)^p$ and ϵ (emiss) is $\epsilon_o(\lambda_o/\lambda)^q$, then for simple geometry ($g_1 = g_2$) the grain temperature is:

$$T_g = \left[\frac{\gamma(4+p) \sum_{n=1}^{\infty} n^{-(4+p)}}{\gamma(4+q) \sum_{n=1}^{\infty} n^{-(4+p)}} \left(\frac{hc}{k\lambda_o} \right)^{q-p} \frac{L_\star}{16\pi\sigma_{SB} r^2} T_\star^p \right]^{\frac{1}{4+q}} \qquad (2)$$

where σ_{SB} is the Stefan-Boltzmann constant.

Grain size has a strong effect on the grain temperature. Arbitrarily large (blackbody) grains with efficient emission at all wavelengths will have the lowest temperature at a given location, while very small grains (like interstellar grains) with inefficient emission at all relevant wavelengths will have the highest temperature.

The most important consequences of this regarding the "Vega phenomenon" are: (1) infrared emission can be proven to be due to grains illuminated by the star in question if the temperature and spatial scale of the emission are consistent, and (2) an estimate of the typical grain size can be made from measurements of the emission temperature and scale. For example, if the grains are much larger than the peak wavelengths of both the absorbed and emitted spectra (blackbody grains), then p=q=0 and Eq. (2) reduces to:

$$T_g = 278\, L_\star^{\frac{1}{4}}\, r_{\rm AU}^{-\frac{1}{2}}\ {\rm K} \qquad (3)$$

where $L_\star$ is in units of $L_\odot$, 3.9×10^{33} erg s^{-1}. The temperature can also be calculated using the source *angular* scale and the *apparent* brightness of the central star. For example, Eq. (3) for blackbody grains can be rewritten as:

$$T_g = 88\, \theta^{-\frac{1}{2}}\, 10^{0.10(4.75-m_v-B.C.)}\ {\rm K} \qquad (4)$$

where θ is the grain distance from the star in arcsec, m_v is the star's visual magnitude, and B.C. is the bolometric correction in magnitudes for the star's type (see, e.g., Allen 1976).

A grain much larger than the peak wavelength of the incoming stellar radiation but much smaller than the peak wavelength of the grain thermal emission would have efficient absorption ($p = 0$) but inefficient emission (q>0). If $p = 0$ and $q = 1$, one obtains:

$$T_g = 468\, L_\star^{\frac{1}{5}}\, r_{\rm AU}^{-\frac{2}{5}}\, \lambda_o^{-\frac{1}{5}} {\rm K} = 186\, \theta^{-\frac{2}{5}} 10^{0.08(4.75-m_v-B.C.)}\, \lambda_o^{-\frac{1}{5}}\ {\rm K} \qquad (5)$$

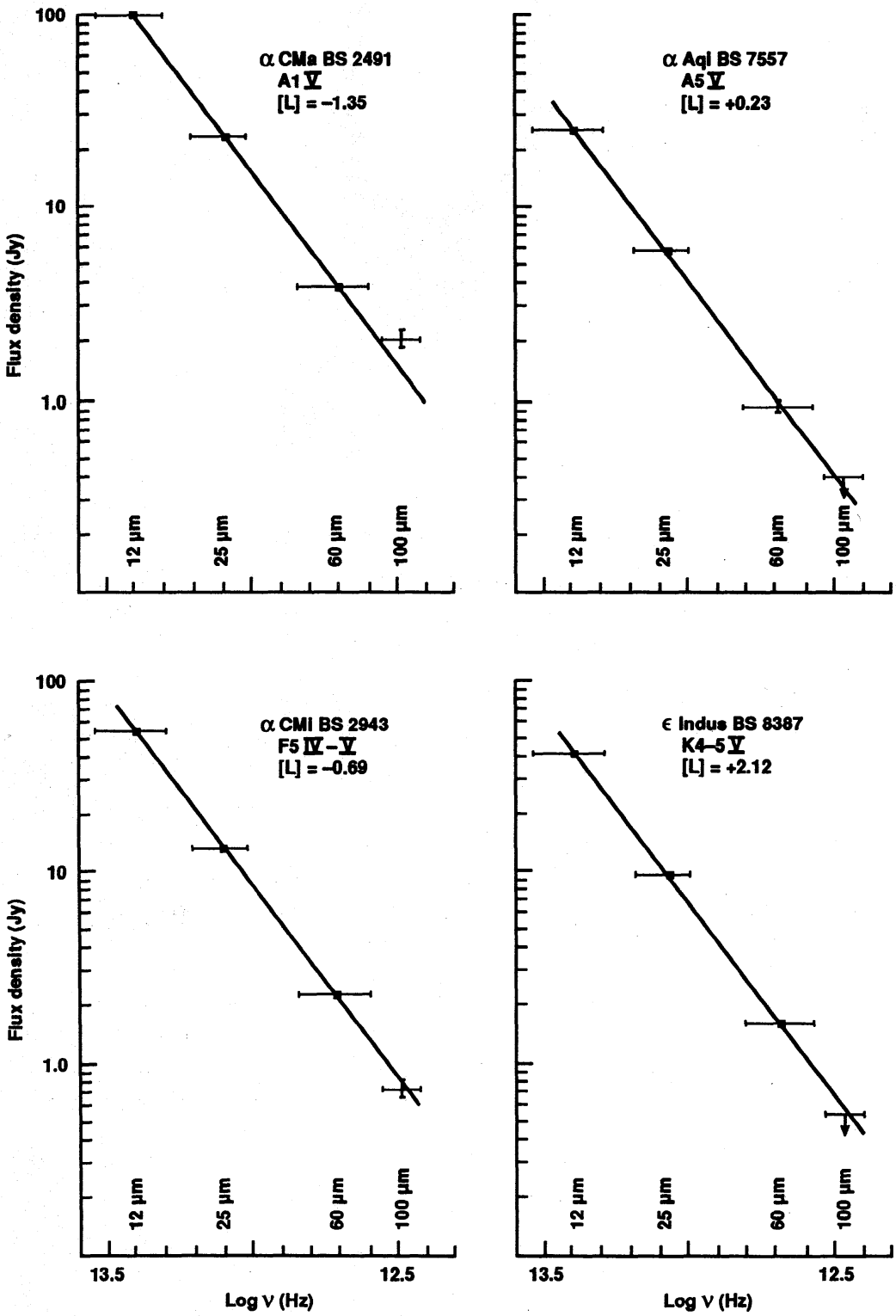

Figure 2. Comparison of spectral energy distributions of four stars of similar spectral types to those in Fig. 1, but with little or no far-infrared excess emission.

where λ_o is in μm.

ISM grains are small enough that they both absorb and emit stellar radiation inefficiently as well as emit inefficiently. Assuming p=q=1.5, one obtains:

$$T_g = 636\, L_\star^{\frac{2}{11}}\, r_{\rm AU}^{-\frac{4}{11}} \left(\frac{T_\star}{T_\odot}\right)^{\frac{3}{11}} {\rm K}$$
$$= 275\, \theta^{-\frac{4}{11}}\, 10^{(0.80/11)(4.75-m_v-B.C.)} \left(\frac{T_\star}{T_\odot}\right)^{\frac{3}{11}} {\rm K} \qquad (6)$$

where $T_\odot$ is 5770 K.

The temperatures described in Eqs. (1)–(6) are physical temperatures of the grain material. The received grain emission spectrum will be affected by the radiative efficiency for $\lambda > \lambda_o$ such that:

$$F_\nu = \epsilon_\nu B_\nu \left[T_g(r,a)\right] \Omega = \left(\frac{\xi a \nu}{c}\right)^q B_\nu \left[T_g(r,a)\right] \Omega \qquad (7)$$

where ξa represents the critical wavelength λ_o and Ω is the solid angle subtended by the total of the geometric cross sections of the grains.

Assuming an optically thin disk and single-size grains, the flux density received at the Earth from a system of grains is:

$$F_\nu = 2\pi \times 10^{23} \int_{r_1}^{r_2} \sigma_o \left(\frac{r}{r_o}\right)^\gamma \left(\frac{\xi a \nu}{c}\right)^q B_\nu \left[T_g(r,a)\right] \frac{r\,{\rm d}r}{D^2}\ {\rm Jy} \qquad (8)$$

in Janskys [= 10^{-26} W m^{-2} (Hz bandwidth)$^{-1}$], where $B_\nu[T_g(r,a)]$ is in cgs units, D is the distance to the system, and the amount of material in the disk is expressed as a face-on fractional geometric surface density $\sigma(r)$, cm^2/cm^2, following a power law in radius with exponent γ. The face-on optical depth for such a disk would be $\tau_\perp(r,\nu) = \sigma(r)(\xi a \nu/c)^q$. The volume density distribution producing a spectrum would be $n(r) \propto r^{\gamma-1}$.

Equation (8) can be converted to an expression which allows integration over temperature rather than radius, concentrating most of the "modeling power" in those regions where the temperature and thus the thermal emission is largest (Artymowicz et al. 1989):

$$F_\nu \propto \int_{T_{\rm min}}^{T_{\rm max}} \epsilon_\nu B_\nu(T_g) y(T) T^{-\kappa} \frac{{\rm d}T}{D^2} \qquad (9)$$

where $\kappa = 4$ for blackbody grains (Eq. 3) or $\kappa = 3$ for "intermediate" sized grains (Eq. 5), and $y(T(r)) \propto r\sigma(r)$.

A spectrum falling more steeply than an RJ slope at long wavelengths may indicate the grain spatial distribution rather than a limit on grain size. Conversely, for some spatial distributions an RJ slope can be produced by an ensemble of grains substantially smaller than the wavelengths of observation.

Combining Eq. (3) for blackbody grains with Eq. (8), assuming $r_1 = 0$ and $r_2 = \infty$ but also assuming that total optical depth along the disk plane is small, there are exact solutions for the spectral energy distribution if $\gamma > -2$. These have the form:

$$F_\nu \propto \lambda^{2\gamma+1}. \tag{10}$$

A spectrum declining faster than an RJ slope results from a disk spatial distribution with $\gamma < -1.5$ even if the grains are assumed arbitrarily large. Note that this is an idealization since total grain area, mass, and optical depth actually diverge for an infinite distribution with $\gamma > -2$. A realistic spatial distribution would have finite inner and outer radii (the inner radius perhaps fixed by the temperature of grain evaporation) and would therefore emit a spectrum falling below the simple power law at both short and long wavelengths.

III. RESOLVED EXAMPLES: α LYR, α PSA, AND β PIC

Examples of the "Vega phenomenon" which have been definitely spatially resolved are the regions around the three stars α Lyr, α PsA and β Pic, although Aumann (1991) may have found a measurable extent for ϵ Eri as well. The three resolved systems deserve special attention because resolution allows structural models and discussion of origins and evolution. This section will discuss observational data, models and interpretations of these systems.

Characteristics of the stars are shown in Table I. All three systems are well within the range of accurate trigonometric parallax distance determinations. A comparison of the visual/near-infrared colors of these stars ("obs": Koornneef 1983*a*; Campins et al. 1985) to the average colors for main sequence stars of their spectral types ("std": Koornneef 1983*b*) in columns 7 and 8 demonstrates that these three have no significant near-infrared excesses. The expected main sequence lifetimes in the last column corresponding to the estimated masses are interpolated from Iben (1967).

A. General Analyses of the "Big 3"

1. IRAS Discovery. Table II presents the photospheric and excess flux densities in the IRAS bands from "pointed" observations (Gillett 1986). The uncertainties include estimates of absolute calibration uncertainty; the relative photometric uncertainties are only a few percent. The 12 μm IRAS measurements are close to photospheric for α Lyr and α PsA but β Pic has a significant excess even at that wavelength.

The possibility that the observed excesses include substantial line emission can be rejected. The infrared continuum of α Lyr is smooth across the range of wavelengths ($\leq$13 μm) over which it has been carefully compared to standards with no far-infrared excess (Witteborn and Cohen, personal communication). Reports of weak visual wavelength emission lines and variability of α Lyr (Johnson and Wisniewski 1978, and references therein) have not been confirmed and are likely due to difficulties in observing such a bright object

1993prpl.conf.1253B

TABLE I
Stellar Characteristics

	BS #	Spectral Type	T_e	m_v	B.C.	obs $V-L$	std $V-L$	dist	$L_\star$	$M_\star$	Expected Lifetime
α Lyr	7001	A0V	9700 K	+0.02	−0.40	0.00	0.00	8.1pc	$60L_\odot$	$2.5M_\odot$	4×10^8 yr
α PsA	8728	A3V	8800	+1.15	−0.23	+0.15	+0.21	7.0	13	2.0	7×10^8
β Pic	2020	A5V	8200	+3.85	−0.12	+0.38	+0.36	16.4	6	1.5	2×10^9

TABLE II
Photometric Characteristics

	IRAS Flux Densities, Janskys				Single temperature Fit to Spectrum	
	12 μm excess (photosphere)	25 μm excess (photosphere)	60 μm excess (photosphere)	100 μm excess (photosphere)	$T_{B.B.}$	Bolometric $f \equiv L_e/L_\star$
α Lyr	0.0 ± 0.8 (28.0)	2.75 ± 0.5 (6.45)	8.2 ± 0.5 (1.1)	7.1 ± 0.8 (0.4)	89 K	2×10^{-5}
α PsA	0.3 ± 0.8 (11.3)	1.4 ± 0.2 (2.6)	9.35 ± 0.5 (0.45)	11.1 ± 1.1 (0.2)	72	8×10^{-5}
β Pic	1.6 ± 0.1 (1.2)	10.1 ± 0.5 (0.3)	18.8 ± 0.9 (0.05)	11.2 ± 1.0 (0.02)	108	3×10^{-3}

optically and finding suitable reference standards. Recent 1-μm-resolution spectrophotometry of β Pic near 10 μm shows that a small amount of silicate line emission is present (Telesco and Knacke 1991).

The excess flux densities at 25 to 100 μm can be fit fairly well in all three cases by Planck distributions with single temperatures listed in column 6 of Table II. A single-temperature fit implying a single radial location for the material is of course only schematic. As discussed previously, many combinations of radial density and grain size distributions can produce a spectrum which resembles portions of a Planck distribution. In the case of β Pic, accounting for all of the 12 μm excess (excluding the weak line emission) in the simplest way requires addition of a second hotter component.

Fractional luminosities f of the excesses relative to the stars are presented in the last column of Table II. The optical depth of grains along a radial line from the star to infinity is $\tau \sim f/\sin i$ if the grains are in a "wedge" or "flaring" disk with thickness proportional to radius and opening angle $2i$. The range of fractional luminosities for these three stars is surprising: f for β Pic is more than 1 order of magnitude larger than for α PsA and 2 orders larger than for α Lyr. Note that the fractional luminosity of the material around β Pic is 4 orders of magnitude larger than for the zodiacal dust in our solar system (Sec. VI).

IRAS profiles of these three sources show widths that are significantly wider than profiles of point sources. Figure 3 compares the average of 12 scans at 60 μm across α PsA, the largest of the three resolved sources, with a point source profile which is a combination of 24 scans of α Boo and β Gru.

Table III presents intrinsic 60 μm source sizes for the three resolved cases estimated from simple deconvolution (Gillett 1986). Note that these are characteristic scales of the strongly emitting regions but are not limiting outer diameters of the sources; substantial amounts of cooler material may lie at larger distances. In the cases of α Lyr and α PsA the sizes given are the largest of values measured along several scan position angles. These can be used to estimate diameters of circular figures seen in projection as ellipses (Sec. III.A.6). In the case of β Pic the infrared source sizes along two orthogonal directions have been de-projected using the disk orientation angle seen in optical images (Sec. III.B.1).

2. α Lyr as Prototype: Large Grains In Orbit. Explanations for infrared excesses other than an optically thin collection of orbiting grains can be eliminated by arguments from the first α Lyr IRAS paper (Aumann et al. 1984), *which also should be considered for all candidate analogs to α Lyr found in IRAS data.* Note that points (c), (d) and (e) depend on successful spatial resolution of the infrared emitting region.

(a) Plasma (free-free) emission, e.g., from a hot wind: the excess is well fit by a Planck function and rises in flux density between 12 and 60 μm, inconsistent with a thin or partially thick free-free spectrum which would have $f_\nu \propto \lambda^{-2}$ to λ^0;

(b) Chance alignment with background interstellar cirrus: the source

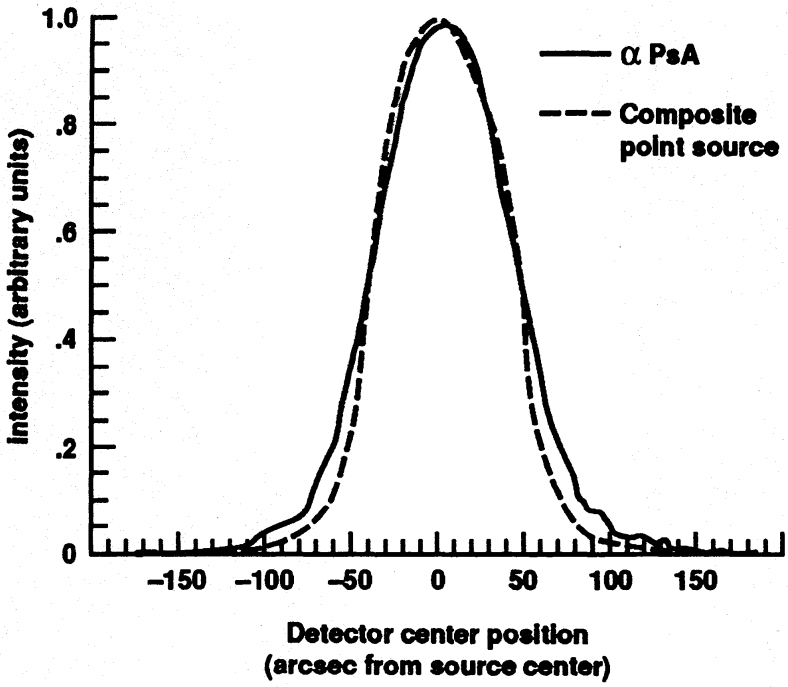

Figure 3. Comparison of IRAS 60 μm scan profiles of α PsA, the most extended of the "Big 3," with a composite of several point sources. The scans were made at 1/2 the all-sky-survey scan rate with a sampling interval of 3.6 arcsec. Scan widths represent a combination of detector FOV, detector response time, telescope diffraction and intrinsic source width; the FWHM is equal to the 90 arcsec detector width parallel to the scan direction ("in-scan"). The profiles are normalized to 1 at their peaks, which makes the broader source appear narrower above the FWHM points. Irregularities in the α PsA profile wings indicate the noise level (data provided courtesy of F. Low, F. Gillett, G. Neugebauer, J. Good and H. Aumann).

temperature of 89 K is much warmer than even unusually warm cirrus knots (Low et al. 1984);

(c) Chance alignment with an 89 K infrared object: the 60 μm source scale of 29 arcsec is quite consistent with heating of grains many μm in size by the star (Eqs. 4 and 5) and the centroid of the far-infrared source is found to be within 2 to 3 arcsec of the star's position, strongly indicating that the emission must be from grains around α Lyr;

(d) A single optically thick blackbody, either a cool self-luminous companion or a single object heated by Vega: its diameter from the flux and temperature would be 0.2 arcsec, much smaller than the observed diameter of the source;

(e) Emission from ordinary circumstellar/ISM grains around α Lyr with efficiencies approximately proportional to $\lambda^{-1.5}$: the diameter of such a shell with the observed color temperature would be almost 2000 arcsec (Eq. 6);

(f) Emission from ordinary grains in a shell around a low-luminosity companion close to the line of sight to the primary star: based on normal ISM grain efficiencies, the shell optical depth would be 4×10^{-3} and the luminosity

TABLE III

Source Sizes, Estimated Grain Sizes, Total Area, and Mass

	Source Diameters, Arcsec			Single-Size Grain Models			
	Observed 60 μm	Hypothetical B.B. Grains	Hypothetical ISM Grains	Grain Size, λ_o, μm	Total Grain Area, cm^2	Minimum Mass, $M_\oplus$	"Maximum" Mass, $M_\oplus$
α Lyr	29	21	1800	80	1×10^{27}	2×10^{-3}	9×10^{2}
α PsA	36	17	1300	27	3×10^{27}	2×10^{-3}	2×10^{3}
β Pic	26	1	180	1	3×10^{29}	7×10^{-3}	4×10^{4}

of the companion would be 0.4 $L_{\odot}$. Such a companion would be detectable as a close optical double, but none is observed (see, e.g., Hanbury Brown et al. 1974);

(g) Large grains condensing in a stellar wind flowing from Vega: a mass-loss limit of $\dot{M} < 3.4 \times 10^{-10}$ $M_{\odot}$ yr^{-1} was obtained for α Lyr from radio and ultraviolet measurements (Hollis et al. 1985, and references therein). Even with optimistic assumptions about the carrying capacity of a wind with α Lyr's metallicity, i.e., all the elements except H and He condensed into grains and a wind speed just above escape velocity, this upper limit on mass loss precludes enough mass in a continuous spherically symmetric wind to be carrying the minimum grain mass of 10^{-8} $M_{\odot}$ (Table III) across the indicated range of radii. The crucial conclusion that the grains must be in orbit around the star rests on (1) the impossibility of interstellar grains being found at the observed radii and temperatures, and (2) inconsistency of mass loss limits with the amount of solid material observed.

Regarding mass loss from the other prototypes: β Pic's shell is like typical A–F shells in showing no overt signs of mass loss like asymmetric or violet-displaced lines (Slettebak and Carpenter 1983), but precise evaluation of mass-loss limits for β Pic is complicated by transient absorption line events (Sec. III.B.5). α PsA has ultraviolet absorption lines which may be from circumstellar gas (Kondo and Bruhweiler 1985) although an analysis of optical Na I and Ca II lines (Hobbs et al. 1985) indicates otherwise. Assuming for a limit that all of the column density tabulated in Bruhweiler and Kondo (1982) represents material in a spherically symmetric wind with solar abundance, fractional ionization $X(Mg^{+}) = 0.01$, v_{∞} of 15 km s^{-1}, and purely gravitational deceleration, then the mass-loss rate from α PsA is less than 10^{-9} $M_{\odot}$ yr^{-1}.

3. Grain Sizes and Total Grain Mass. Columns 3 and 4 in Table III show the source sizes expected from the source temperatures if the grains are blackbody grains (Eq. 4) or ISM grains (Eq. 6). The actual grains in all three cases can be judged to be smaller in size than 100 μm but also clearly larger than ISM grains because the observed source sizes lie between these extremes. The grains around α Lyr appear to be the largest, approaching blackbody size, while the grains around β Pic appear to be relatively small.

Typical grain sizes can be estimated by assuming the grains are intermediate-sized ($\epsilon < 1$ across the IRAS bands) and calculating a best fit to the observed source size and 25 to 100 μm flux densities. Resulting grain size parameters ($\lambda_o \sim a$) are presented in column 5 of Table III. The total grain areas in column 6 of Table III are geometric cross sections. The values of grain size and total area depend on the assumed value of emissivity exponent q but the relative ranking of the three systems is preserved if the same q is used for each. Note that the amount of material is anti-correlated with the mass and luminosity of the central stars.

The quality of the fits of these single-size grain models to the observed spectra are not great. It is more likely that the grains have a range of locations and sizes, but this exercise gives some indication of effective or typical grain

sizes. The calculated grain size for α Lyr for $q = 1$ appears to be nearly large enough to violate the assumption implicit in Eq. (5) that most of the emission takes place at wavelengths larger than λ_o. A solution for α Lyr with blackbody grains yields nearly the same grain area.

The mass associated with the circumstellar grains is of primary importance and unfortunately is also uncertain. The grain size distribution slope and maximum sizes are not constrained by the IRAS observations. Minimum total masses derived with the assumptions that all the grains have size $a = \lambda_o$ and density 1 g cm^{-3} are presented in column 7 of Table III (1 $M_\oplus = 3 \times 10^{-6}$ $M_\odot = 6 \times 10^{27}$ g). These masses are quite small; note especially in the case of α Lyr that 2×10^{-3} $M_\oplus$ of 80 μm grains can produce a far-infrared signal which overpowers the star's flux and is easily detectable at stellar distances. In the case of β Pic the lower limit to the grain mass is approximately consistent with solar composition and an upper limit on neutral gas mass (Sec. III.B.4).

A maximum grain mass presented in the last column of Table III can be estimated by assuming: (1) collision fragmentation equilibrium size distribution $n(a) \propto a^{-3.5}$ (Dohnanyi 1969); (2) minimum size $a_{\min} = \lambda_o$; (3) maximum size $a_{\max} = 1000$ km estimated from the gravitational instability in a thin dust disk at 100 AU (Goldreich and Ward 1973; Greenberg et al. 1984); and (4) density of 5 g cm^{-3}. These values are larger than the total mass of the planets in our solar system (450 $M_\oplus$) and scale with the assumed maximum size as $a_{\max}^{1/2}$. The grain upper mass limit for β Pic is 0.1 $M_\odot$. The grain population that contains most of the surface area and is most easily detected does not represent the population containing most of the mass in this distribution: half of the total area is contained in grains smaller than 4 times the minimum size, while half the mass is contained in grains larger than 1/4 the maximum size.

Note that the deduced maximum mass is quite sensitive to the size distribution exponent: assuming a power law a^{-4} rather than $a^{-3.5}$ produces "maximum" mass estimates smaller by a factor of 10^4. Grain size distributions caused by mechanisms differing from collisions, such as sublimation of icy bodies, seem to give size distributions differing from $a^{-3.5}$ in our solar system (see, e.g., Kyte and Wasson 1986).

4. Inner and Outer Boundaries. An important fact provided by the spectral energy distributions of these objects is that they have relatively empty central regions (Gillett 1986). This conclusion is based on consideration of maximum grain temperature determined by minimum wavelength of excess flux. If in Eq. (8) the outer boundary radius $r_2 \rightarrow \infty$, then the entire disk emission can be characterized by the value of the inner boundary radius r_1. Table IV presents estimates of inner boundary radii for each of the three systems constrained by the hottest IRAS color temperature and assuming grain sizes from Table III. The solutions differ significantly depending on whether a flat or steep spatial distribution is assumed. Only in the case of β Pic is there independent information about the actual spatial gradient ($\gamma \sim -1.7$ at r greater than about 65 AU; Sec. III.B.1).

TABLE IV
Inner Boundary Radii

	γ	r_1	T_g(max)
α Lyr	0.0	—	—
	−1.7	26	119
α PsA	0.0	30	104
	−1.7	67	75
β Pic	0.0	20	199
	−1.7	38	154

These calculations show that the grain number density in these three systems cannot increase monotonically toward the stars or even be constant with radius. Instead, there must be central regions of relatively low density. These central "voids" have sizes similar to each other and also similar to the planetary region of our solar system. Note that this analysis finds that the amount of material at $r < r_1$ was undetectable with IRAS but it may not be zero, and there is not necessarily a sharp boundary at r_1. One conclusion of Aumann et al. (1984) was that a hypothetical hot grain component around α Lyr with $T = 500$ K could have up to 10^{-3} of the grain area in the 90 K component and not violate the limit on excess at 12 μm. Because PR radiation drag (Sec. V.B.2) would act quickly to fill in the voids, grain removal mechanisms such as ice sublimation, radiation pressure expulsion of small collision fragments, or gravitational perturbations are probably required to prevent a warm dust signature. Better photometry at infrared wavelengths much shorter than the emission peaks would further define the inner structure of these systems and the processes controlling the location of the grains.

The ability of infinite spatial distributions to yield positive or negative spectral slopes has been discussed. The IRAS data therefore do not allow specification of *outer* boundary radii for these systems. IRAS sensitivity to outlying material would have been limited by detector field of view and grain temperature. The IRAS field of view at 100 μm corresponds to roughly 1500 by 2500 AU at the distance of α Lyr and 3000 by 5000 AU at β Pic. Material colder than about 30 K has an emission peak beyond the long wavelength cutoff of the IRAS 100 μm band and would be difficult to detect without substantial optical depth. That temperature corresponds to distances of about 1000 AU from α Lyr and 2300 AU from β Pic for the model grain characteristics in Table III.

5. Is the β Pic System Really a Disk? We are likely to be viewing the β Pic system from near the star's equatorial plane because the star's projected rotation velocity is above the mean for main-sequence stars of its spectral type (Table V). Is it possible that the linear structure seen in the coronagraph images is not a disk of orbiting grains? Could it instead

TABLE V

Stellar Rotation and IRAS Source Orientation

	Mean v sin i for Spectral Type, km s^{-1}	Observed v sin i, km s^{-1}	Apparent Grain Disk Inclination, i, degrees
α Lyr	145	15	30^{+15}_{-30}
α PsA	135	100	>70
β Pic	125	139	>80

represent equatorial mass loss or even bi-polar jets emanating from a post-main-sequence star as Herbig (1989*b*) speculated based on the disk optical appearance and Slettebak's (1975) classification of the central star as a sub-giant? The argument that the observed system must actually be a disk of orbiting material is provided by Paresce and Artymowicz (1989), which we summarize:

(a) An equatorial flow capable of reaching the great distances of the observed disk can be rejected because the escape velocity from the β Pic atmosphere is about 500 km s^{-1} but the observed rotation rate is 139 km s^{-1};

(b) The bipolar jet hypothesis can be rejected because there is little resemblance between bipolar nebulae and the β Pic disk in terms of scale, mass, grain temperature, expansion velocity, lifetime, or molecular content;

(c) The central "void" would require that the grains condense at much colder temperatures than in all other known examples of grain condensation in stellar winds;

(d) Such a jet would need to be directed by another substantial disk that would necessarily also lie close to our line of sight to the star, yet no such disk is observed;

(e) There are no obvious spectroscopic signs of mass loss (Slettebak and Carpenter 1983);

(f) The surface brightness declines rapidly as r^{-4} or steeper, but material on an escape trajectory decelerating gravitationally and presenting a "wedge" in projection (Sec. III.B.1) would instead have scattering surface brightness following $r^{-2.5}$ (r^1 increasing viewing path length $\times$ $r^{-1.5}$ volume density decrease $\times$ r^{-2} decrease of input photons).

6. Source Morphologies and Stellar Rotation. Previously described analyses by Gillett (1986) of IRAS 60 μm in-scan and cross-scan profiles of α Lyr yields minimum and maximum source scales of 25 and 29 arcsec, interpreted as roughly FWHM of the surface brightness distribution. Because these scans were made along a number of position angles, it appears that this source is nearly circular in projection. The same analysis for α PsA yields a scale of 36$\pm$2 arcsec along position angle 29° W of N, but less than 13 arcsec perpendicular to that direction. In this case there is only one scan axis and therefore size estimates only along two position angles. The actual source shape for α PsA could be between two extremes: (1) elliptical, with axial

ratio less than 13/36 and major axis along the IRAS scan direction, or (2) a one-dimensional source lying along a position angle 10° E of N.

The IRAS spatial information on β Pic is of lower quality but is consistent with a one-dimensional source oriented like the optical disk. A careful analysis of the scattered light isophotes (Artymowicz et al. 1989) shows that the disk inclination to the plane of the sky is greater than 80° (Sec. III.B.1).

These source shapes provide crucial information about the true location of the grain material relative to the rotation axes of these stars. Table V compares the observed (projected) stellar rotation velocities (Uesugi and Fukuda 1970) with the average (projected) rotation velocities for stars of the same spectral types (Schmidt-Kaler 1982, and references therein). This is statistical evidence that the star α Lyr is nearly pole-on to us, that β Pic is nearly equator-on to us, and that α PsA lies between those extremes. There is also independent evidence from detailed spectral line analysis (Gray 1986) that what we see in the case of α Lyr is the pole of a rapidly rotating star.

The inclination angles of disks which would result in elliptical projections with the observed aspect ratios are in the last column of Table V. This comparison of the rotational orientation of the three stars with the projected shapes of the regions containing the grains is the basis for concluding that the material is probably arranged as disks in the stellar equatorial planes.

7. IRAS Followup. A number of investigators have extended the original IRAS results on source sizes and spectral energy distributions for the three resolved systems. Harvey et al. (1984) confirmed the α Lyr excess from the Kuiper Airborne Observatory (KAO) and measured a source size at 47 and 95 μm consistent with, but marginally larger than, the IRAS values. Lester et al.'s (1990) KAO 100 μm characteristic size for α PsA is in agreement with Gillett (1986) along the major axis, and they find evidence for some emission at least 240 AU (35 arcsec) from the star. Aumann (1991) re-analyzed IRAS slow-scan observations of α Lyr, α PsA, β Pic, and other stars assuming Gaussian intrinsic source profiles and found sizes like Gillett's (1986) except an upper limit twice as large as Gillett's for α PsA's minor axis. Early KAO photometry by Harper et al. (1984) showed flux density from α Lyr at 193 μm well below an extrapolation of the IRAS 25 to 100 μm color temperature. Becklin and Zuckerman (1990) found a similar result for α Lyr and β Pic (but not α PsA) at 450 and 800 μm using the 15 m James Clerk Maxwell Telescope (JCMT). They also noted that the excess flux from α PsA was stronger at an offset of 16 arcsec (one beamwidth) from the star than in a beam centered on the star, which they interpreted as direct confirmation of the central "void" inferred from the spectrum. Becklin and Zuckerman modeled the emission from the three systems as due to emission from material at one temperature (i.e., no spatial distribution) and thus interpreted their and Harper et al.'s flux-density shortfalls relative to IRAS extrapolations as evidence of: (1) smaller grain sizes ($a << \lambda_{obs}$); and (2) lower total dust masses, than previously published. However, rapidly declining long-wavelength spectra can also be produced by some spatial distributions (Sec. II.B). Chini et al. (1990) used the

30 m Instituto de Radioastronomia Millimetrica (IRAM) telescope and found excesses relative to the stellar photospheres which decrease as $\lambda \rightarrow 1$ mm, but claim an inconsistency exists between their beamsize/flux density/source size information and that of Becklin and Zuckerman (1990). Chini et al. find their results in agreement with the IRAS source sizes.

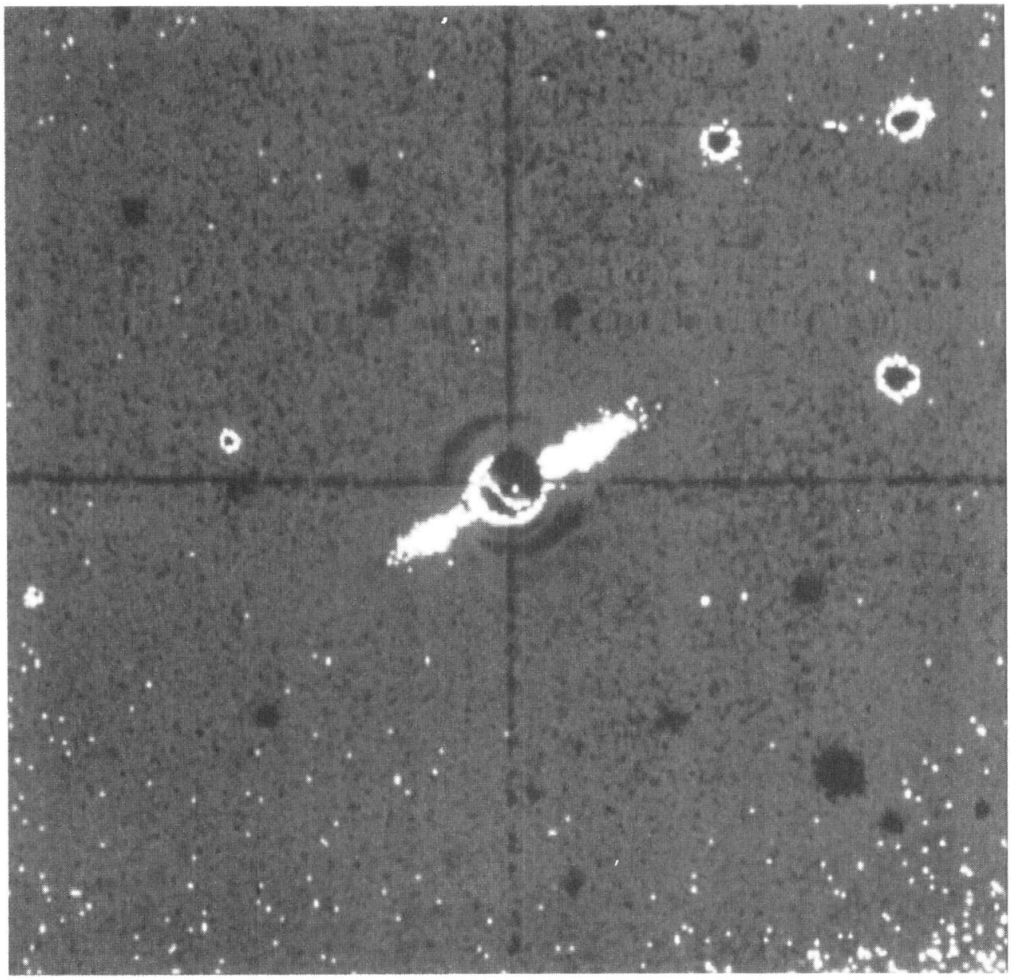

Figure 4. Red (0.89 μm) CCD coronagraph image of the β Pic disk from the 100-inch telescope at Las Campanas. The extent of each wing of the disk is roughly 25 arcsec or 400 AU. Processing involved use of comparison images of α Pic to remove the profile of light scattered in the atmosphere and instrument (figure from Smith and Terrile 1984).

B. Detailed Analyses of β Pic

It has already been noted that β Pic possesses the warmest and proportionately most luminous infrared excess of the "Big 3". Following the IRAS discovery Smith and Terrile (1984) used a CCD coronagraph to detect 0.89 μm (I-band) light scattered by grains in a nearly edge-on disk around the star (Fig. 4). β Pic is the only example which has been so far detected optically because it is by a wide margin the densest main-sequence grain disk within 20 pc (Sec. IV.A.4) and is fortuitously inclined so as to enhance the surface brightness by

roughly an extra factor of 10. β Pic is also nearly unique among these systems in that it exhibits substantial excess emission at wavelengths as short as 10 to 20 μm (Aumann and Probst 1991). β Pic is therefore the object in this class about which most is known and considerable discussion of its properties is warranted.

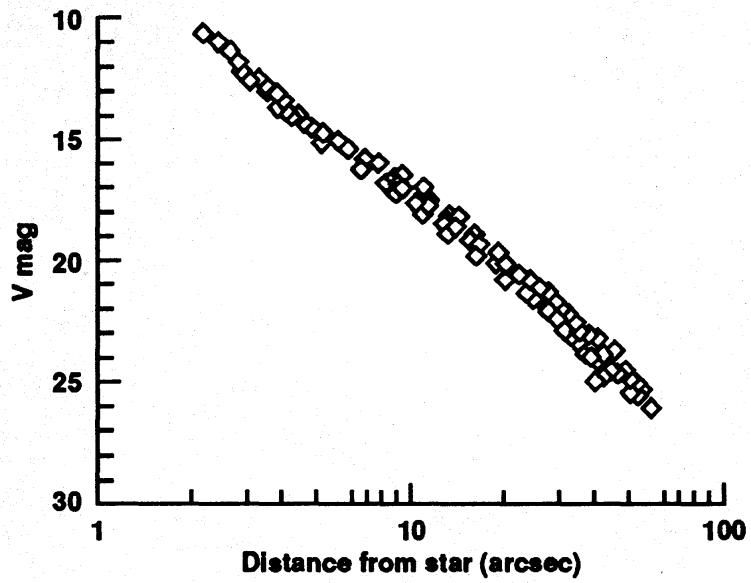

Figure 5. Radial surface brightness distribution in V band of the β Pic disk midplane, both wings plotted together. (Smith and Terrile, unpublished data.)

1. Disk Structure: Optical. The disk was visible beyond the edge of Smith and Terrile's coronagraph mask at $r \geq 6$ arcsec (100 AU) extending about 25 arcsec (450 AU) to the north-east and 20 arcsec to the southwest along a position angle of 30° (Fig. 4). The disk is resolved along its short dimension, with a seeing-deconvolved thickness of 3 arcsec (50 AU) at $r = 350$ AU. The I-band surface brightness is 16th magnitude per square arcsec at 100 AU, decreasing approximately as $r^{-4.3}$.

Subsequent images (Smith and Terrile 1987) show the disk apparently extending inward to radii of a few arcsec and outward to 60 arcsec (1100 AU). The most complete surface brightness profile combining the two "wings" is shown in Fig. 5. The surface brightness fades below present detectability beyond 1100 AU but the disk may well extend farther.

Smith and Terrile's (1984) Fig. 2 implies that there is an asymmetry of the disk involving truncation of the southwest wing and increasing thickness of that wing near its outer terminus. A brown dwarf companion for β Pic was suggested (Whitmire et al. 1988) as a possible cause for such a disturbance of the disk. However, Paresce and Burrows (1987) found no systematic asymmetry in the disk structure in their optical coronagraph images. In fact, asymmetries with both the same *and opposite* sense of that originally proposed

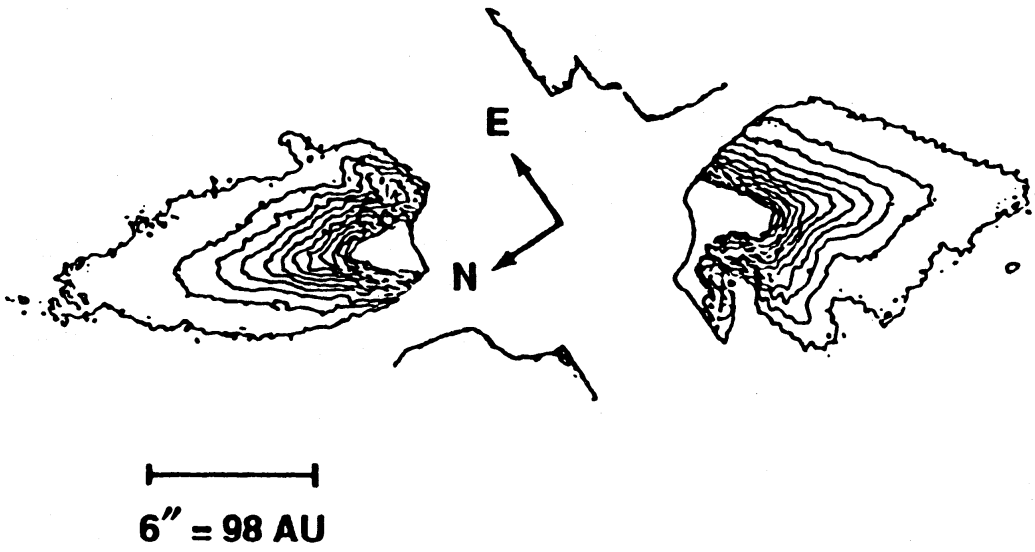

Figure 6. Contour plot of the β Pic disk surface brightness at 0.79 μm. The isophotes are most easily modeled as a "wedge" disk (thickness increasing with radius) convolved with atmospheric seeing (figure from Artymowicz et al. 1989).

can be easily produced by small registration errors in the nontrivial process of reducing coronagraph images using reference star images.

Model pertaining to the specific radii range of 6–15 arcsec (100–250 AU) show that the likeliest structure capable of producing the observed elliptical isophotes (Fig. 6) is a "wedge" disk having an opening angle of about 14° and a presentation angle (versus exactly edge-on) of 10° or less, convolved with terrestrial seeing (Artymowicz et al. 1989). Those model calculations show that the isophotes for a constant thickness disk would be quite different and easily distinguished from a wedge and that the symmetry of the surface brightness distribution is consistent with a scattering phase function similar to that for zodiacal dust (see especially Artymowicz et al. Figs. 1 and 3–7). It is more difficult to distinguish between model isophotes of a wedge versus a very thin, inclined disk. However, the latter hypothesis is rejected because it would require an unlikely scattering phase function more isotropic than Lambert's law.

Given a slightly inclined wedge geometry, the optical depth *perpendicular to the disk plane* is deduced to follow approximately $r^{-1.7}$ for $r \geq 65$–100 AU (Artymowicz et al. 1989,1990). This corresponds to a mid-plane grain volume number density declining approximately as $r^{-2.7}$.

2. Models Combining Optical and Infrared Data. The area corresponding to the infrared luminosity of the entire disk is within a factor of two of the scattering area observed outside coronagraph masks (Artymowicz et al. 1989; Backman et al. 1992). The total grain surface cross-sectional area is related to the scattering area σ_s, the infrared (absorption/emission) area σ_i, and the

albedo $\mathcal{A}$ via:

$$\sigma_{total} = \sigma_s + \sigma_i = \sigma_s/\mathcal{A}. \quad (11)$$

Plausible albedos imply there cannot be much more grain area hiding within the regions obscured in coronagraph images.

The grain temperature in 4 and 8 arcsec fields of view centered on the star is 180 K from observations at 10 and 20 μm if radiative efficiency is assumed to be $\epsilon \propto \lambda^{-1}$ (Telesco et al. 1988; Backman et al. 1992). Because the temperature on these scales is not growing rapidly with decreasing aperture size, one can estimate that the maximum temperature of detectable material is $T_{max}\sim$200 K, which corresponds quite well to the limits in Table IV based on IRAS data.

Models attempting to match both infrared data and results of analyses of optical observations have been calculated by Diner and Appleby (1986), Nakano (1988), Artymowicz et al. (1989) and Backman et al. (1992). All combined optical-infrared models agree on a relatively flat spatial distribution for the grains producing the bulk of the grain thermal luminosity. These models in general show:

1. An outer component corresponding to the disk visible in coronagraph images, extending from $r \leq 100$ AU to $r \geq 1000$ AU with mid-plane grain number density decreasing steeply as $n\sim r^{-3}$; this component emits most of the radiation detected at $\lambda > 20$ μm;
2. A transition region extending approximately from r = 10–100 AU as yet hidden from easy view in coronagraph images, with a lower density and either smaller grains or a less steep spatial gradient than the outer component; most of the radiation at $\lambda < 20$ μm originates from this region;
3. An innermost region with grain area below present detection limits.

Details of the structure in the region hidden by coronagraph masks such as the sizes and properties of the transition region and innermost "void" are not uniquely determined by the available infrared observations (see, e.g., Diner and Appleby 1986). The grain cross-section area in these regions is as little as 1% of the amount there would be if the outer component gradient continued to $r = 0$. The face-on optical depth in the inner component is of order 10^{-4} in contrast to a maximum in the outer disk of a few times 10^{-3}. The physical mechanisms that may contribute to the relatively low density of material in the inner regions of the β Pic disk are discussed in Secs. V.B and C.

The midplane visual extinction Δm based on assumption of a "wedge" structure and following the definitions in equation (8) is:

$$\Delta m_\lambda \sim 1.1\tau_\lambda \sim 1.1 \int_{r_1}^{\infty} \frac{\sigma_o}{\theta r} \left(\frac{r}{r_o}\right)^{\gamma} dr = \frac{1.1\sigma_o}{-\gamma\theta} \left(\frac{r_1}{r_o}\right)^{\gamma} \text{mag} \quad (12)$$

where r_o is a reference radius of 100 AU, r_1 is the radius of the disk inner edge, and θ is the wedge angle ~0.1 rad (Artymowicz et al. 1989). Models with

small grains (Sec. III.B.3) predict the correct infrared spectrum and source size if $r_1 \sim 30$ to 100 AU for the main outer disk component containing most of the optical depth and if $\sigma_o \sim 1\text{–}5 \times 10^{-3}$, yielding $\Delta m \leq 0.04$ mag. This agrees with careful analysis (Paresce 1991; see Sec. V.A below) of β Pic photometry versus new metallicity indices and isochrones showing that the star lies on the zero age main sequence (ZAMS) within the uncertainties involved. Thus, our line of sight through the disk does not suffer significant extinction. The conclusion by Smith and Terrile (1984) that there must be a central cavity of roughly 30 AU radius is therefore only fortuitously correct because their argument was based on an assumption that substantial gray extinction is observed toward β Pic.

3. Grain Properties. The composition and size of the grains around β Pic are significant in comparing this system to our solar system. Grain sizes are necessary input to calculations of grain lifetimes against removal processes discussed in Sec. V.A such as direct radiation pressure expulsion, mutual collisions, collisions with interstellar grains, PR radiation drag, and ice sublimation. Grain lifetimes in turn are crucial to hypotheses of the source and evolution of the grains.

One complication is that the grains are unlikely to have a single size. A steady-state size distribution $n(a) \propto a^{-3.5}$ has been derived from theoretical studies of inelastic collisions and fragmentation processes and compared to observations of asteroids and micrometeoroids (Dohnanyi 1969). This distribution has been adopted in some discussions of the β Pic system (see, e.g., Smith and Terrile 1984; Matese et al. 1987). Model calculations based on observations usually yield a single size parameter, but the relation between such a size and the properties of a realistic size distribution are quite uncertain (see, e.g., Backman et al. 1992).

Scattering properties of the grains will be set in part by their size. Smith and Terrile (1987) and Paresce and Burrows (1987) find that the color of the scattered light is the same as the color of the star within observational uncertainty across the range 0.4 to 0.9 μm. This would indicate grains 1 μm or larger in size. Gradie et al. (1987) have found very red colors for the disk, $V-I \sim 0.6$ magnitudes redder than the the star, also implying a grain size larger than 1 μm. Gledhill et al.'s (1991) optical polarization measurements yield a (model-dependent) size of about 0.25 μm.

As previously discussed, the grain size can be characterized by a comparison of the run of temperatures represented by the thermal spectrum to measurements of the size of the infrared emitting region. Telesco et al. (1988) determined the size of the warmest grains radiating at 10 μm to be 0.1 to 0.4 μm; Backman et al. (1992) find typical sizes of 2 to 20 μm or minimum sizes of 0.05 to 3 μm for the infrared emitters depending on choice of emissivity exponent and spatial gradient.

Artymowicz (1988) has calculated the ratio of radiation pressure forces to gravitational forces acting on small grains in the β Pic system, similar to the work of Burns et al. (1979) for grains of various types in our solar system (Sec.

V.B.1). The deduced minimum stable size for a wide variety of compositions is of order 1 μm, and could be larger if the grains are porous, delicate, or icy. There may also be a size regime (perhaps smaller than $\leq$0.1 μm, depending on composition) below which grains would couple inefficiently to the β Pic radiation field and also be stable. Grains in the range 0.1 to 1 μm should be subject to rapid ejection from the system.

Various groups have thus reported substantially different grain size results, and the disagreements are difficult to interpret. Comparison of the radiation pressure calculation with the optical and infrared observations indicates that the β Pic grain size distribution may not be continuous but may consist of one population smaller and one larger than the size range excluded by direct radiation pressure.

Artymowicz et al. (1989) concluded that the β Pic disk has 9×10^{28} cm^2 of optical scattering cross-section area in the region 100 AU$<r<$500 AU, yielding an albedo of $\mathcal{A} = 0.6$ (Artymowicz et al. 1989) or 0.35 (Backman et al. 1992) for the grains at $r>100$ AU depending on the amount of thermal radiating area attributed to the same region. These albedos are very high compared to small grains found in various parts of our solar system such as zodiacal dust grains ($\mathcal{A} \leq 0.1$; Hauser and Houck 1986) or grains in comet comae ($\mathcal{A} \sim 0.2$; Ney 1982). Even material which is nearly pure ice by mass with carbon added at solar abundance has albedo generally below 0.1 (Clark and Lucey 1984).

4. Spectroscopy of the Classical Shell Gas Component. β Pic has been classified as a shell star because of the presence of strong narrow circumstellar absorption features superimposed on the cores of some of the broad photospheric lines at ultraviolet wavelengths (Slettebak and Carpenter 1983; Kondo and Bruhweiler 1985; Lagrange et al. 1987; Lagrange-Henri et al. 1988) and at visible wavelengths (Slettebak 1975; Hobbs et al. 1985; Vidal-Madjar et al. 1986; Ferlet et al. 1987; Hobbs et al. 1988). The lines involved are listed in Table VI and are transitions from resonance (= ground) or metastable states, signifying gas with low density and temperature relative to the stellar atmosphere. 'I' signifies a neutral species, 'II' singly ionized, and 'III' doubly ionized.

The shell absorption lines in the β Pic spectrum themselves have complex multi-component structures. In general this structure can be decomposed into a strong stable component at the star's 21 km s^{-1} heliocentric radial velocity, plus additional components especially noticeable in the Al III and Mg II lines which are extremely variable in strength and velocity on time scales of days and months and are always redshifted with respect to the stable component (Sec. III.B.5). Both the stable and variable components were recently observed with the Goddard High-Resolution Spectrograph on the Hubble Space Telescope (Boggess et al. 1991).

The stable component may correspond to a "classical" A–F star shell. Detectability of the Ca II 3d and Fe II metastable transitions indicates that the radiation dilution (solid angle subtended by the star) must be $W>10^{-5}$ in

TABLE VI

Shell Lines in the β Pic Spectrum

Line	λ, Å
UV	
Al III resonance	1854
Fe II resonance multiplet	~2600
Fe II metastable	2750
Mg II resonance doublet	2795, 2802
Mg I resonance	2852
VISUAL/FAR-RED	
Ca II K resonance	3934
Na I D2 resonance doublet	5890, 5896
Ca II 3d metastable	8542

order that the rate of depopulation of the lower levels via spontaneous decay be negligible compared to radiative absorption (see, e.g., Viotti 1976). This in turn indicates that the stable lines from ionized gas originate in material at $r \leq 1$ AU. Thus, the presence of β Pic's "classical" shell may be unconnected to the infrared/optical grain disk lying at roughly 10 to 1000 AU. There is no correlation between strength of far-infrared excess and strength of spectroscopic A–F shell indicators (Hobbs 1986; Jaschek et al. 1986), and contrary to Jaschek et al. (1986), the frequency of far-infrared excess in A shell stars is not anomalously high compared to ordinary A stars (Sec. IV.A.3).

Velocity dispersion parameters of $b = 1.8$ km s^{-1} for Na I versus 3.7 km s^{-1} for Ca II K are evidence that the material producing the neutral sodium absorption is connected to the grain disk because it seems to lie farther from the star than the ionized material in the shell. Most of the gas mass around β Pic would be expected to lie in this outer component considering the relative volumes and densities, and would distinguish β Pic from "classical" A–F shell stars. Estimates of the total gas mass (including hydrogen) indicate that it is less than 2 $M_\oplus$, (<0.5% of the mass in our planetary system) (Vidal-Madjar et al. 1986; Hobbs et al. 1988). Model results indicate that the gas near the star is roughly solar-composition but the line strengths imply that the region where the Na is located must be extremely depleted in Ca relative to Na, possibly because the Ca is trapped in grains (Vidal-Madjar et al. 1986). A recent search (Lagrange-Henri et al. 1990) for spectroscopic analogs to β Pic is discussed in Sec. IV.B.

5. Transient Spectroscopic Events: Comet Impacts? Although spectral variability is also found in other shell stars, the unique occasional highly red-shifted absorption events at β Pic have been claimed as evidence of impact of comet-like bodies onto the star (see, e.g., Ferlet et al. 1987; Lagrange-Henri et al. 1988; Beust et al. 1990; Beust et al. 1991). The most dramatic changes occur on time scales as short as an hour for the Al III line and 6 to 8 hours for

the Ca II line. Individual components of the Al III and Mg II lines can reach equivalent widths of 400 and 900 mÅ and velocities of 350 and 300 km s^{-1}, respectively. These velocities are comparable to free-fall speeds at 2–3 $R_\star$. In contrast, the Ca II K variable components never exceed about 40 km s^{-1} red shift. Estimated frequencies of redshifted events for the Ca II K line are 10 to 100 yr^{-1} and 100 to 200 yr^{-1} for the Al III line depending on red shift. Typical velocities and frequencies appear to vary somewhat over the course of years.

A highly developed but not unique explanation for these phenomena is described by Beust et al. (1990,1991). In their model the transient events in the metallic lines are attributed to the passage through the observer's line of sight of infalling asteroids or comets producing clouds of dust grains that are sublimating or evaporating as they approach the star. The amount of absorbing material is equivalent to the complete vaporization of cometary objects several kilometers in diameter. The observed multi-component structure of the time-variable features can be plausibly explained in this scenario as resulting from objects breaking into pieces due to tidal disruption or extreme heating. The ratio of radiation pressure to gravity is a factor of 10 larger for Ca II ions than for Al III and Mg II ions, which is crucial to explaining the large differences in their observed behavior. Their model also includes a planetary mass in the β Pic system that sends the infalling bodies on the inferred trajectories. A complete dynamical simulation described in Beust et al. (1991) is able to fit the spectroscopic data well with only a few free parameters.

A cometary hypothesis is not as far-fetched as it might seem since small Sun-grazing comets that are totally disrupted in the ensuing collision are known to occur in our own solar system as often as 10 times per year (Michels et al. 1982). It is therefore an interesting possibility that the younger and perhaps more crowded β Pic system is host to many active comets.

IV. SEARCHES FOR VEGA-LIKE SYSTEMS: SURVEYS AND INTERPRETATION

A. Infrared Searches

The statistical properties of the IRAS Point Source Catalog (PSC) including detectability and characteristic far-infrared properties of various types of objects are discussed by Chester (1985). The IRAS Faint Source Survey (FSS) released in September 1990 consists of coadded survey data and is thus 2 to 3 times as sensitive as the PSC, but avoids the galactic plane and does not contain sources detected only at 100 μm.

1. IRAS Limitations in Observations of Stars. Normal main-sequence photospheres are difficult targets of study in IRAS data for the following reasons:

(a) Stellar photospheres of different types all have approximately RJ spectra and are nearly indistinguishable in the IRAS data, with [12]–[25], etc.

colors close to 0.0 mag. As a corollary, cool main-sequence *physical* companion stars are essentially undetectable with IRAS—the maximum possible color excess E(V-[12]) due to a main sequence binary companion to any main sequence primary is roughly 0.2 magnitudes.

(b) IRAS was only slightly more sensitive than the human eye to sources with stellar temperatures; the PSC 12 μm completeness limit of $\sim$0.4 Jy corresponds to visual magnitude +5.0 for A and +7.5 for G main-sequence stars (d<30 pc!).

(c) Most stars cooler than the Sun detected by IRAS are giants; the dividing line between detection of mostly dwarfs versus mostly giants is at B–V $\sim$0.75 (approximately spectral type G5) (Waters et al. 1987).

In the absence of circumstellar material one would therefore expect that only a few nearby and bright main-sequence stars would be found in the IRAS data and that even these would not be detected beyond 12 μm.

Unlike binary companions, *background* stars are capable of producing substantial excesses in IRAS observations of nearby stars in measures of V-[12], V-[25], etc. In a groundbased 2.2 μm photometric study of the IRAS fields of view around approximately 60 candidate stars with substantial V-[12] excesses, Aumann and Probst (1991) found that only 2 (β Pic and ζ Lep) had true intrinsic 12 μm excess and the rest were caused by red background stars. This implies that the phenomenon of far-infrared excesses around main-sequence stars is usually limited to temperatures below about 200 K.

IRAS discovered that the sky is covered with low-temperature emission from the general ISM, now called infrared "cirrus," which is concentrated toward the galactic plane. The usually extended cirrus emission includes concentrations which sometimes mimicked the characteristics of a point source in IRAS data processing. One of the warmest such sources found at high galactic latitude and discussed by Low et al. (1984) has a color temperature of 34 K. A source with color temperature less than 40 K is most significantly detected in the 100 μm band in IRAS data. Thus, sources associated by position with nearby stars but having T_c<40 K, and also excesses detected only in the 100 μm band, are possibly due to background cirrus. This is more likely statistically at low galactic latitudes. One way to eliminate candidate Vega-like sources caused by background cirrus would be improved spatial resolution in future infrared instruments which might show a cold source to be an extension of a larger structure or not centered on the star in question.

The far-infrared color typical for galaxies and infrared galactic components (HII regions, planetary nebulae, parts of molecular clouds and star forming regions) of $f_\nu(25)<f_\nu(60)$ (Chester 1985) also describes the prototype main-sequence circumstellar sources. However, infrared galactic components are strongly concentrated toward the galactic plane and thus would likely produce only a few spurious candidates. External galaxies, especially starburst galaxies, can have spectra and fluxes similar to the Vega-like sources (Helou and Beichman 1991) and far-infrared sizes of order 10 arcsec, so it is at least possible that some Vega-like candidates could be produced by a galaxy lying

in the background of a star, although the number density of sufficiently bright galaxies versus IRAS 60/100 μm detector field of views of 7 to 15 square arcmin makes for agreement with subject. Again, future comparison of source centroids with star positions can help eliminate this possibility.

Finally, reflection nebulae have been found to emit in all 4 IRAS bands, generally with $f_\nu(12) < f_\nu(25) < f_\nu(60) < f_\nu(100)$ after removal of direct flux from the illuminating star (Sellgren et al. 1990). Some of the 60/100 μm ratios are not far from 1 and thus are similar to the circumstellar disk prototypes. This similarity should not be surprising because the β Pic disk is in a sense a reflection nebula. Characteristics which might distinguish orbiting material from ISM grains warmed by a luminous star might be: symmetric versus asymmetric source shape and/or angular scale too small for emission involving small ISM grains. Once again, spatial resolution superior to that available with IRAS may be needed to distinguish normal reflection nebulae from Vega-like systems.

2. *IRAS Data on Typical Main-Sequence Stars.* Waters et al. (1987) and Cohen et al. (1987) summarize PSC data on objects in the Bright Star Catalog (BSC) (Hoffleit and Jaschek 1982). Both papers present typical V-[12], V-[25], etc. colors for a range of spectral types and luminosity classes and confirm the expectation that there are no significant flux *deficits* relative to expectations of RJ or slightly steeper slopes; disturbances to photospheric colors are exclusively *excesses*. An independent check by Graps (personal communication) confined to luminosity class V found V-[12] colors similar to Waters et al.'s means for all spectral types. These colors are about 0.1 mag redder than predicted by stellar atmosphere models.

Figure 7 presents the median IRAS 12/25 μm flux density ratios versus spectral type for the 670 BSC stars of luminosity classes IV, IV–V, and V detected in both bands (Graps, personal communication). These continuum slopes are quite similar to those found for Gliese catalog (nearby) stars (Backman and Gillett 1987) and for SAO stars (Stencel and Backman 1991).

Among A and early F stars, even typical stars have modest 25 μm excesses with median T_c cooler than $T_{\rm eff}$ by several thousand degrees. Note that the ratio for α Lyr is exactly at the median for types B9-A1, yet approximately 25% of the 25 μm flux density in that case is known to be excess from grains. For these types, 50th percentile falls closer to the blue end of the distribution, because the population includes only a few stars with substantial excesses. Median (50th percentile) late F, G and early K stars fall near the average of the range, and the range is consistent with IRAS photometric uncertainty, implying that few of these stars have detectable excess at 25 μm compared to 12 μm. Typical B IV–V stars have substantially redder colors than stars of later types and 50th percentile falls nearer the red end of the ranges, approaching the colors of a free-free plasma emission spectrum. This is consistent with the typical B star having a free-free excess but with a blue tail in the population toward stars with more nearly photospheric colors.

3. *Published Surveys and Present "Master List."* A number of searches

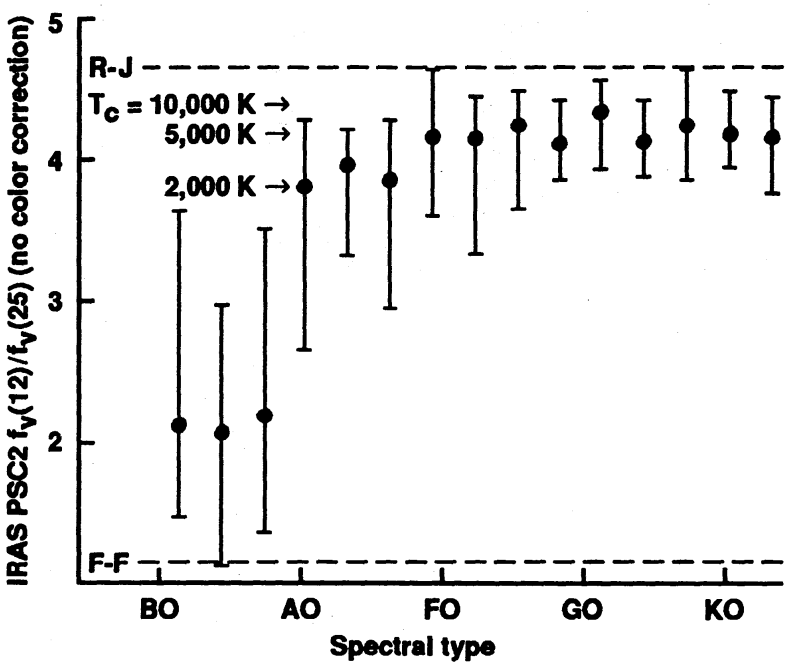

Figure 7. Median IRAS 12/25 μm flux density ratios (raw, i.e., without bandwidth color corrections) vs spectral type for main-sequence stars in the Yale Bright Star Catalog detected in both bands. Stars with giant or supergiant companions were excluded. There were few enough main-sequence stars later than K4 that they were also excluded. The type bins represent combinations of groups of 3 subtypes, i.e., the median labelled A0 is for B9, A0, and A1 stars considered together. The error bars represent the range from 25th percentile to 75th percentile. The R-J line at the top represents the color of a blackbody of infinite temperature. The F-F line at the bottom represents the color of pure free-free (plasma) emission.

have been conducted for examples of stellar far-infrared excesses. Aumann (1985) examined PSC data on stars with $d<25$ pc and found 12 stars with galactic latitude $|b_{II}|>10$ deg having [12]–[60] >1.0 mag, defined there as Vega-like, including the three resolved prototypes. The fact that the ones with excess are mostly A–F stars was recognized as probably due to a luminosity selection effect. Sadakane and Nishida (1986) examined PSC data on BSC members and found 12 more Vega-like stars using criteria identical with Aumann's (1985), again mostly A-F stars with *no lack of excesses in binary systems,* which may be very significant information about the mechanisms for forming these grain clouds. One of the stars, λ Boo, is known to be metal deficient, which is interesting in light of the low metallicity of β Pic (Sec. V.A), and raises the issue of composition of the circumstellar grains. Coté (1987) examined PSC data on BSC B and A stars and found 24 examples of infrared excess, some of which were also noted in the previous studies. Twenty-one of these cases are attributed by the author to dust emission, 3 to free-free emission.

Odenwald (1986*a*, *b*) examined PSC data on G stars of all luminosity

TABLE VII

Compendium of Published Lists of Main-Sequence Stars with Far-Infrared Excess

	HR	Type	V	References[a]
49 Cet	451	A3V	5.6	SN, WW
DM+19 279	493	K1V	5.2	B2
τ Cet	509	G8V	3.5	B1, B2
γ Tri	664	A1Vnn	4.0	Co
τ^1 Eri	818	F6V	4.5	Au, B2
τ^3 Eri	919	A4V	4.1	B2
α For	963	F8V	3.9	WW
ϵ Eri	1084	K2V	3.7	Au, B1, B2
π^1Ori	1570	A0V	4.7	SN
HD 31648		A2ps	7.7	Ja
κ Lep	1705	B9V	4.4	SN
DM+79 169	1686	F6V	5.0	Au, Ho, WW
HD 34700		G0	8.7	WW
HD 35187		A2	8.2	WW
ζ Lep	1998	A3Vn	3.6	B2, Co
δ Dor	2015	A7V	4.4	Co
β Pic	2020	A5V	3.8	Au, B2, Co, Ja
HD 41511	2148	A2s	4.9	Ja
ψ^5 Aur	2483	G0V	5.3	B2
HD 53143		K0V	6.8	WW
B Car	3220	F5V	4.8	B2
HD 233517		K2	8.7	WW
	3314	A0V	3.9	Co
δ Vel	3485	A1V	2.0	B2, Co, WW
β UMa	4295	A1V	2.4	Au, Co
HD 98800		K5V	8.6	WW
Ross 128		M5V	11.1	B1
β Leo	4534	A3V	2.1	Au, B2, Co WW
HD 121384	5236	G6IV-V	6.0	WW
λ Boo	5351	A0p	4.2	SN
σ Boo	5447	F2V	4.5	B2
HD 135344		A0V	8.7	WW
γ Tra	5671	A1V	2.9	Co
α CrB	5793	A0V	2.2	Au, Co, Ho
HD 139614		A7V	8.0	WW
HD 139664	5825	F5IV-V	4.6	WW
HD 142666		A3	8.2	WW
HD 144432		A9+F0 V	8.4	WW
σ Her	6168	B9V	4.2	SN, Co
	6297	A5IV-V	5.7	Co

TABLE VII (cont.)

	HR	Type	V	References[a]
HD 155826	6398	F7+G2 V	6.0	WW
DM-24 13337	6486	A3m	4.2	B2
μ Ara	6585	G3IV-V	5.2	B2
γ Oph	6629	A0V	3.8	SN, Co
	6670	F3IV-V	5.8	SN
HD 169142		B9V	8.3	WW
α Lyr	7001	A0V	0.0	Au, B2, Ho, Co
	7012	A5IV-V	4.8	Co
61 Cyg	8085	K2+K5 V	5.2	B1, B2
δ Equ	8123	F5+G0 V	4.7	B2
DM-47 13928	8323	G2V	5.6	Au, WW
α PsA	8728	A3V	1.2	Au, B2, Co
	8799	A5V	6.0	SN
HD 221354		K0V	6.7	WW

[a] References: Au = Aumann 1985 (Gliese+Woolley catalogs; PSC+coadds); B1 = Backman et al. 1986 (d<5 pc stars; survey coadds + pointed obs.); B2 = Backman and Gillett 1987 (Gliese subset; survey coadds); Co = Cote 1987 (BS catalog B+A stars; PSC); Ho = Hobbs 1986 (shell stars; PSC); Ja = Jaschek et al. 1986 (shell stars; PSC); SN = Sadakane and Nishida 1986 PASP 86, 685 (BS catalog; PSC); WW = Walker and Wolstencroft 1988 (HD catalog; PSC-extended sources).

classes and found strong infrared excesses mostly from dusty shells around supergiants, but also at least one case of a main sequence excess. Johnson (1986) found warm excesses around some K dwarfs, most of which are classified as T Tauri stars. Jaschek et al. (1986) examined PSC data on 19 Ae/A shell stars comparable in optical spectral qualities to β Pic and found 8 with strong far-infrared excess. This is similar to the frequency of excesses among normal A stars in samples of nearby stars (Sec. IV.A.4). There appears to be no clear correlation between the optical and infrared properties of shell and emission line stars.

Walker and Wolstencroft (1988) selected HD stars (m_v>10) with PSC 60/100 μm flux density ratios similar to the prototypes. In addition, they examined evidence of the extent of the emission via the IRAS data "confusion" flag, which was set when a source was seen by 3 detectors in one waveband, nominally requiring a size of at least 20 arcsec. The data were then analyzable in terms of grain size and total mass. Some of the objects discovered in this survey have stronger far-infrared fluxes than the prototypes, and since these HD stars are in general dim the fractional luminosities (optical depths) in some cases approach 1, substantially different from the prototypes. A search for CO emission (Walker and Butner 1991) from some of these stars did not detect any molecular material other than probable background emission.

Backman et al. (1986) combined groundbased near-infrared photometry

with IRAS pointed observation ("AO") data on stars within 5 pc and found several examples of weak excess which had been missed at the sensitivity level of the PSC. One of those stars, Ross 128, is the only M dwarf so far known to have a Vega-like excess. α CMa (Sirius) was found to have a weak 100 μm excess, but the characteristics seem to exclude emission from orbiting grains, as confirmed by Chini et al. (1990) with mm-wave measurements.

Table VII is a "master list", a union of lists of main-sequence (luminosity class IV, IV–V, and V) stars found to have far-infrared excesses. Because the selection criteria and procedures were not uniform and the IRAS data used had various sensitivities, this list is of somewhat mixed quality.

Backman and Gillett (1987) and Aumann (1988) showed by examining coadded survey photometry of nearby stars that the phenomenon of far-infrared excesses (a) may be the rule rather than the exception for main-sequence stars, (b) appears in all spectral types, and (c) is not restricted to stars of young age. The implication that our solar system might also have a cool excess when viewed from outside is considered in Sec. VI.D.3.

4. Bright Star Catalog and Gliese Catalog Surveys. Table VIII presents a complete list of BSC main-sequence stars found to have Vega-like far-infrared excesses, as defined below. There is some overlap between this list and the "master list" in Table VII. The original sample consisted of all BSC stars in luminosity class V with detected flux at 12 μm and having no higher-luminosity class companion. In case of dimmer companions, the system is listed by the primary's spectral type. IRAS PSC2 data were used and all infrared sources within 60 arcsec of the star position corrected for proper motion to 1983.5 were accepted.

It was found in a plot of $f_\nu(25)/f_\nu(60)$ versus $f_\nu(12)/f_\nu(25)$ (Fig. 8) that the three prototypes α Lyr, α PsA, and β Pic spanned a broad stretch of the diagram, and a number of objects were found to lie in the same stretch. Stars of spectral class O or Be were found to lie often in a region with $f_\nu(25)/f_\nu(60) > 1$ and $f_\nu(12)/f_\nu(25) < 2.5$ which contains the locus of a purely free-free spectrum and were rejected as having excesses likely due to plasma emission. Stars with detected flux at 100 μm but with $f_\nu(60)/f_\nu(100) < 0.2$, i.e., $T_c < 30$ K, were excluded as being likely due to background cirrus. Finally, stars with $f_\nu(25)/f_\nu(60) > 4.0$, i.e., $T_c > 500$ K, were excluded; over that wavelength range, those colors do not differ significantly from photospheric colors. These criteria in combination are essentially equivalent to a search for excesses most prominent at 60 μm.

Note the two trajectories in Fig. 8 which show the loci of points corresponding to: (a) a system like β Pic if the disk luminosity is decreased relative to the star from its actual value of 2×10^{-3} toward 1×10^{-5}, approaching the upper right of the diagram where the colors of a pure stellar photosphere lie; and (b) a system like α PsA if the disk luminosity is increased relative to the star from its actual value of 8×10^{-5} toward 1×10^{-2}, approaching the locus of β Pic. This indicates that the different loci of β Pic and α PsA in this color-color plot simply represent different fractional grain luminosities but

TABLE VIII

Bright Star Catalog Main-Sequence Stars with Vega-like Far-Infrared Excesses

HR	Type	V	IRAS fqual	F_ν, Jy 12μm	Excesses, Jy 25μm	60μm	100μm
123	B8Vn	4.73	3133	0.43	0.00	0.96	2.44
189	B5V	5.67	1333	0.28	0.41	1.01	2.03
241	B9.5V	6.21	3332	0.28	0.21	3.87	11.18
287	A3V	6.47	1133	0.25	0.00	0.76	2.70
333	A3V	5.62	3131	0.26	0.00	0.34	0.00
451	A3V	5.63	3233	0.33	0.33	1.99	1.90
506	F8V	5.52	3331	0.82	0.14	0.81	0.00
533	B1.5V	5.52	2332	0.26	0.76	2.29	3.74
664	A1Vnn	4.01	3332	1.07	0.21	0.81	0.83
811	B7V	4.25	3333	0.66	0.32	1.32	1.76
818	F6V	4.47	3322	1.88	0.20	1.55	4.98
890	B7V+B9V	5.03	3223	0.53	0.56	3.10	14.07
963	F8V	3.87	3321	4.11	−0.02	0.11	0.00
1074	B1V	5.90	1321	0.25	0.41	1.07	0.00
1082	A3V	6.38	1131	0.26	0.00	0.58	0.00
1084	K2V	3.73	3333	9.52	0.28	1.23	1.73
1144	B8V	5.64	1231	0.47	0.48	2.97	0.00
1151	B8V	5.76	3333	0.42	1.04	4.66	10.90
1307	B8Vn	6.23	3333	1.15	6.16	26.27	37.19
1399	B7V	5.53	1333	0.46	1.07	5.77	16.13
1415	B3V	5.55	3333	0.35	0.98	2.60	3.48
1448	A2Vs	5.68	1131	0.39	0.00	0.54	0.00
1570	A0V	4.65	3121	0.73	0.00	0.42	0.00
1686	F6V	5.05	3221	1.14	−0.04	0.23	0.00
1719	B5V	6.13	1132	0.30	0.00	1.02	2.73
1798	B2Vn	6.25	1331	0.26	0.61	1.54	0.00
1808	B5V	5.42	1233	0.43	0.41	1.57	3.59
1839	B5V	4.20	3121	0.56	0.00	0.55	0.00
1868	B1V	5.34	3323	0.38	1.86	7.50	6.16
2015	A7V	4.35	3332	1.39	0.04	0.45	1.11
2020	A5V	3.85	3333	3.46	8.22	19.75	11.23
2124	A2V	4.12	3333	1.50	0.63	3.20	2.75
2161	B3V	6.66	1131	0.25	0.00	0.57	0.00
2522	B6V	5.39	3333	0.43	1.52	4.58	5.67
2806	O9V	6.43	1331	0.25	0.56	1.43	0.00
3415	B3V+B3Vn	5.26	1131	0.51	0.00	0.51	0.00
3720	A1V	5.29	3233	0.47	0.07	1.26	2.74
3927	A0V	5.72	1131	0.29	0.00	0.68	0.00
4295	A1V	2.37	3331	4.80	0.24	0.43	0.00

4534	A3V	2.14	3331	6.97	0.44	0.88	0.00
4732	B3Vn	4.82	3131	0.27	0.00	0.79	0.00
5250	B8VpShell	5.15	2123	0.24	0.00	1.07	2.16
5336	B4V	5.06	3332	0.31	0.63	6.04	10.04
5793	A0V	2.23	3331	5.92	0.31	0.50	0.00
5902	B2.5V	5.03	3231	0.56	0.26	0.63	0.00
5933	F6V	3.85	3331	3.85	−0.08	0.24	0.00
6168	B9V	4.20	3321	0.96	0.02	0.22	0.00
6211	B8V	6.46	1131	0.52	0.00	1.06	0.00
6532	B9.5V	6.42	1132	0.25	0.00	0.69	1.28
6533	A1V	5.62	3133	0.30	0.00	0.46	1.23
6629	A0V	3.75	3331	1.41	0.17	1.23	0.00
7001	A0Va	0.03	3333	41.56	1.08	7.75	7.12
7030	B8V	6.41	1133	0.25	0.00	0.83	1.43
7035	B5.V	5.83	1133	0.66	0.00	3.33	8.49
7329	A0Vn	5.05	3331	0.54	0.35	0.51	0.00
7474	B3V+B3V	5.17	2332	0.68	1.37	5.08	7.70
8323	G0V	5.58	3221	0.81	0.02	0.21	0.00
8549	B2V	6.46	1133	0.25	0.00	1.01	1.33
8728	A3V	1.16	3333	18.21	0.45	8.25	10.91
8854	B0Vn	6.53	3321	0.60	0.79	13.68	0.00

not fundamental differences in disk structure or the mechanism of far-infrared emission. The region of the diagram these trajectories cross is interpreted as the region of Vega-like excesses.

A study made by Backman and Gillett (1987) examined coadded IRAS photometry of 134 stellar systems from the Gliese Catalog (Gliese 1969; Gliese and Jahreiss 1979). The sample was limited to stars of spectral types A–K, luminosity classes V and IV–V, trigonometric parallax $\pi_t \geq 0.045$ ($d < 22$ pc), and color temperatures above 35 K. This study contrasts with the aforementioned Bright Star survey in that the sample was defined by a flux density limit at 12 μm, with the result that a greater proportion of later-type stars were included.

Those stars with significant excesses at 25, 60, or 100 μm with color temperatures above 35 K are listed in Table X. Significance was defined as greater than 3 times the rms noise in the off-source scan baseline. The summed luminosity of components listed by Gliese (1969) was used in calculating the fractional cloud luminosities in column 11. Table IX lists as a function of spectral type an estimate of the sample distance limit (reciprocal of 25th percentile trigonometric parallax), the number of stars in the sample, the fraction of sample stars with significant excesses, and the fraction of sample stars with significant excesses stronger than a fractional luminosity of 2×10^{-5}, approximately equivalent to α Lyr.

The possible meaning of the statistics in Table IX is that there is no strong dependence on spectral type when frequencies of far-infrared excesses

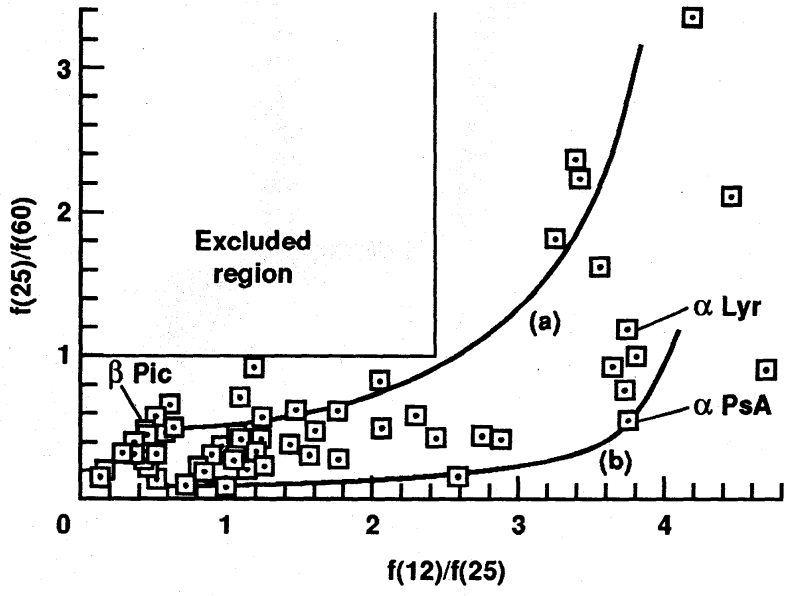

Figure 8. IRAS color-color diagram for main-sequence stars in the Yale Bright Star Catalog. The colors of the three prototype objects are indicated. The two trajectories respectively show the range of colors which the β Pic and α PsA disks would have if all other disk parameters were kept constant while the optical depth was varied. The "excluded" region contains the color of pure free-free emission.

TABLE IX

Far-Infrared Excesses in Gliese Catalog Subsets

Spectral Type	N	Excess $>3\sigma$	Excess $\tau \geq 2 \times 10^{-5}$	Approx. limit (pc)
A	22	41%	18%	20
F	51	10%	10%	18
G	39	10%	8%	15
K	22	14%	14%	7

are compared by fractional luminosity rather than by significance of IRAS detection. Similar results are reported by Aumann (1988). The frequency of far-infrared excesses around A stars at this sensitivity limit is near 50%; it may be that a more sensitive instrument than IRAS will find that fraction approaching 100%. Note also in column 12 of Table X that there are several stars with ages approaching the age of our Sun determined from photometric isochrones (Varsik 1987), lithium abundances (Simon et al. 1985), or emission-line strengths (Duncan 1981). This implies that the Vega phenomenon is not limited to proto-stellar or proto-planetary contexts.

B. Optical Spectroscopic and Coronagraph Searches

Lagrange-Henri et al. (1990) have undertaken a comprehensive spectroscopic survey for β Pic analogs. Since β Pic has both an infrared excess and a

1993prpl.conf.1253B

TABLE X

Gliese Catalog Stars with Far-Infrared Excesses

	Gliese Number	Spectral Type	25 μm Excess (Jy)	e/σ_e	60 μm Excess (Jy)	e/σ_e	100 μm Excess (Jy)	e/σ_e	T_c	τ	Age (Gyr)
68.0	DM+19 279	K1	0.10	1.7	0.11	3.4	0.38	2.9	85	7.1e-5	
71.0	τ Cet	G8	0.06	0.7	0.08	2.1	0.42	6.0	76	1.2e-5	3.5
111.0	τ^1 Eri	F6	0.17	3.9	0.89	35.6	3.65	22.7	62	2.2e-4	2.2 ± 1.6
121.0	τ^3 Eri	A4	0.02	0.8	0.04	1.6	0.15	3.4	75	7.5e-6	
144.0	ϵ Eri	K2	0.29	3.9	1.33	41.7	2.27	41.6	74	9.7e-5	
167.1	γ Dor	F0	0.05	2.2	0.21	9.3	0.21	4.1	83	3.0e-5	
217.1	ζ Lep	A3	0.68	15.4	0.40	12.9	< 0.11	—	139	7.1e-5	
219.0	β Pic	A5	9.05	194.1	20.44	363.4	13.15	115.3	106	2.4e-3	
245.0	ψ^5 Aur	G0	0.11	2.6	0.43	8.9	0.53	2.4	81	1.7e-4	3.8
248.0	α Pic	A5	0.13	3.5	0.00	0.1	< 0.19	—	79	9.2e-6	
297.1	B Car	F5	0.04	2.0	1.76	51.8	3.05	16.9	52	3.5e-4	4.5 ± 1.1
321.3	δ Vel	A0	0.03	0.4	0.29	6.9	< 0.02	—	63	2.8e-6	
364.0	DM-23 8646	G0	0.12	2.8	0.13	5.4	0.24	3.0	98	7.2e-5	2.6
448.0	β Leo	A3	0.41	5.5	0.77	14.9	0.63	7.0	109	1.9e-5	
557.0	σ Boo	F2	0.06	2.2	0.09	3.5	< 0.06	—	83	2.3e-5	2.0 ± 1.5
673.1	DM-24 13337	A9	0.15	1.3	1.02	2.9	11.48	5.9	52	2.9e-4	
691.0	μ Ara	G5	0.22	7.3	0.08	1.1	< 0.96	—	67	1.0e-4	
721.0	α Lyr	A0	1.14	3.4	7.85	114.7	8.89	48.1	74	1.5e-5	
820.0	61 Cyg	K5	0.38	5.1	0.57	5.0	2.38	1.9	77	1.5e-4	
822.0	δ Eql	F8	0.15	3.8	0.07	2.2	0.48	4.9	88	5.4e-5	6.4 ± 1.0
881.0	α PsA	A3	0.34	2.3	8.66	157.2	11.95	109.3	58	5.0e-5	

shell spectrum, they searched 57 candidates that had at least one of those two attributes for the telltale signature of narrow, mostly redshifted and possibly variable circumstellar absorption lines of Ca II and Na I. Although a few (especially HR 10, 2174, 8519 and 9043) had some similarities or were remarkable in some way, none in the sample were found to resemble β Pic in detail.

Coronagraph surveys based on lists of IRAS excesses and/or shell spectra have been made separately by Brahic, Smith and Terrile, and Burrows and Paresce. The latter team examined 20 of the objects in Lagrange-Henri's list mentioned above, and found no disk detectable at radii of 6 arcsec from the stars to an I-band surface brightness limit of about 18 mag arcsec^{-2}. This limit is roughly 2 mag fainter than the β Pic disk, but null results are not surprising considering that β Pic's grain optical depth and orientation are so exceptional.

V. TIME SCALES, DYNAMICS, AND EVOLUTION

A. Ages of The "Big 3"

The metallicities of α Lyr and α PsA are close to solar. Their ages on the Green et al. (1987) revised Yale isochrones are 4×10^8 and 2×10^8 yr, respectively, with uncertainties of roughly 30%. The derived age for α Lyr is near the end of the stage of core hydrogen burning for its mass, and in fact that star is a factor of 3 to 4 times brighter than its ZAMS luminosity.

The indicated metal abundance for β Pic from a new calibration of Geneva photometry (Kobi and North 1990) is $\log_{10}$[M/H]=-0.6 ± 0.3, or 1/4 of solar, rather depleted with respect to normal nearby stars of early spectral class. Fundamental parameters of $R_\star = 1.2$ R$_\odot$ and $M_\star = 1.5$ M$_\odot$ are found, both slightly lower than typical A5 dwarfs but within a plausible range. The ZAMS bolometric magnitude from the Green et al. isochrones for $Z = 0.004$, $Y = 0.2$, $T_e = 8200$ K is $M_{bol} = 2.80\pm0.15$ mag ($1\ \sigma$) versus an observed value from its parallax, V magnitude, and bolometric correction of 2.63. β Pic's age can be estimated to be about 100 Myr, above but close to the ZAMS. The most evolved position on the Yale isochrones allowable (considering the range in possible helium and metal abundances) corresponds to an age of 200 Myr, about 10% of the main sequence lifetime of a 1.5 M$_\odot$ star (Paresce 1991).

B. Intrinsic Grain Removal Processes

Radiation pressure, particle collisions, and ice sublimation are processes which can remove or destroy grains orbiting stars. Their time scales offer clues to the source and evolution of the grain material. Individual processes will be discussed separately in the next sections, followed by discussion and comparison of their rates at inner and outer radii in the three prototype systems.

1. Radiation Pressure Expulsion. A simple derivation of the overpressure ratio δ of radiation to gravitational forces acting on a grain near a star assuming

spherical black ($\mathcal{A} = 0$) grains of radius a is:

$$\delta \equiv \frac{F_{\rm rad}}{F_{\rm grav}} = \left(\frac{3}{16\pi cG}\right)\left(\frac{L_\star}{M_\star}\right)\left(\frac{1}{a\rho}\right) = \left(\frac{0.57}{a_{\mu m}\rho}\right)\left(\frac{L_\star}{\rm L_\odot}\right)\left(\frac{\rm M_\odot}{M_\star}\right). \quad (13)$$

The value of δ is inversely proportional to grain size in this simple treatment. For a given value of grain density there will be one size for which $\delta = 1$, defining a minimum stable or "blowout" size for grains released at rest which depends only on the central star's luminosity and mass. Both forces depend on r^{-2} so their ratio δ has the same value at all locations for a given grain and all regions will be cleared equally well. Grains are propelled beyond radii of 10^3 AU on free-fall time scales of order 10^4 yr by this means. Column 2 of Table XI presents the "blowout" size for each of the three systems. It is interesting that this size is comparable to the typical or abundant grain sizes estimated in Table III, as if this process provides lower limits to grain size distributions weighted toward the smallest grains.

A more careful treatment of radiation pressure effects (Burns et al. 1979) including grain albedo and radiative efficiency shows that there is a maximum value in our solar system of $\delta \sim 0.5$ at a grain size of about 0.5 μm (close to the peak wavelength of the Sun's radiation) for most realistic grain materials. Grains smaller and larger than that size are more stable against ejection, meaning there is no unstable size for grains released at rest in our system. One can approximately scale Burns et al.'s results to other stellar systems with an increase of overpressure by a factor of $(L_\star/\rm L_\odot)(\rm M_\odot/M_\star)$ and a shift of the grain size of maximum overpressure to smaller sizes by a factor of $T_\star/\rm T_\odot$. Artymowicz (1988) employed a similar analysis for the case of β Pic. The general expectation for stars with the luminosities of the three A stars is an excluded grain size range between about 1/30 and 1/2 times the simply calculated "blowout" size.

2. Poynting-Robertson Radiation Drag. Particles stable against radiation pressure ejection are subject to the PR effect in which incoming radiation in the moving frame of the grain has a component that always opposes the grain velocity. This causes grains orbiting in a radiation field to spiral toward their orbit center even if the orbit center and the radiation source are not the same. The orbit decay time due to PR drag (see, e.g., Burns et al. 1979) is:

$$t_{PR} = \left(\frac{4\pi a\rho}{3}\right)\left(\frac{c^2r^2}{L_\star}\right) \text{cgs} = 7.1 \times 10^2 a_{\mu m}\rho r_{\rm AU}^2\left(\frac{\rm L_\odot}{L_\star}\right) \text{yr}. \quad (14)$$

An important characteristic of PR drag is that it is guaranteed to apply to all stably orbiting grains of any composition in any optically thin situation whereas other processes such as mutual collisions or ice sublimation may not apply in some cases.

3. Grain Collisions. The mutual collision time scale is approximately:

$$t_{\rm coll} \sim \frac{t_{\rm orb}}{8\sigma(r)} \sim \frac{r_{\rm AU}^{\frac{3}{2}}}{8\sigma(r)}\left(\frac{\rm M_\odot}{M_\star}\right)^{\frac{1}{2}} \text{yr} \quad (15)$$

where $\sigma(r)$ is the fractional surface density as in Eq. (8). This expression assumes that each orbiting grain encounters the full surface density roughly twice per orbit as it oscillates perpendicular to the disk plane and that the collision cross section is 4 times the cross-sectional area of individual grains to include tangential collisions.

Collisions can be assumed to result in destruction rather than accretion because even tangential collisions at relative speeds greater than 0.1 km s^{-1} (10^8 erg g^{-1}) should result in catastrophic fragmentation (see, e.g., references in Lissauer and Griffith 1989). The relative velocity of grains due to their motion perpendicular to the plane of a disk is approximately $V_z \sim iV_{\rm orb}$, where $2i$ is the opening angle of the disk subtended at the star. For example, for β Pic with an opening angle of about 0.1 rad and $M_\star = 1.5$ $M_\odot$, $V_z > 0.1$ km s^{-1} at $r < 1000$ AU. Most fragments from such high-speed collisions involving small grains would likely be smaller than the "blowout" size and be rapidly ejected from the system.

Grains of various sizes will move at different orbital speeds for the same orbit because the radiation force reduces the effective potential. The range of orbital speeds resulting from this effect for grains between 1 and 10 times the "blowout" size would also imply relative speeds greater than the collisional destruction threshold of 0.1 km s^{-1} throughout the relevant radii ranges even if motions perpendicular to the disks are unexpectedly small.

4. Ice Sublimation. The time scale for sublimation of pure water ice grains can be estimated from expressions in Isobe (1970):

$$t_{\rm subl} = 1.5 \times 10^{-12} a\rho \frac{10^{2480/T_g}}{T_g^{7/2}} \text{yr} \qquad (16)$$

where T_g is the grain temperature. This rate is an extremely powerful function of temperature; i.e., for temperatures of 90 to 120 K, Eq. (16) can be approximated by:

$$t_{\rm subl} \sim 10^6 a_{\mu m} \left(\frac{T_g}{100\text{K}} \right)^{-55} \text{yr}. \qquad (17)$$

A more complete treatment can be found in Lien (1990), including the result that "dirty ice" grains have a much shorter sublimation time scale than pure ice at a given location.

5. Comparison of Grain Removal Time Scales, and Mass-Loss Rates. Columns 4–6 of Table XI contain the time scales for each process at inner boundaries and outer locations in the models of the three systems using grain sizes from Table III and assuming grain density of 1 g cm^{-3}. The PR decay time would increase linearly with increased density. The inner boundary radii are for the $\gamma = -1.6$ case. The outer positions considered correspond roughly to the optically traced extent of the β Pic disk. The face-on optical depths $\sigma(r_1)$ for Eq. (15) can be approximated by the fractional luminosity f in Table III. Time scales labelled ∞ are much greater than 10^{10} yr.

TABLE XI

Grain Removal Processes

	Blowout Size, μm	r_1, AU r_2, AU	Removal Time Scales, yr t_{PR}	t_{coll}	t_{subl}
α Lyr	14	26	2×10^5	5×10^5	9×10^5
		1000	3×10^8	5×10^{10}	∞
α PsA	4	67	6×10^6	6×10^5	∞
		1000	1×10^9	3×10^9	∞
β Pic	2	38	2×10^5	8×10^3	4×10^{-4}
		1000	1×10^8	2×10^8	∞

A number of conclusions can be drawn from this information and a comparison with the stellar lifetimes and ages in Table I and Sec. V.A:

1. The grain lifetimes are shorter than the stellar main sequence lifetimes throughout the systems to $r \sim 1000$ AU.
2. The grain lifetimes are so short at the inner boundaries that the grains must be either continually replenished from some reservoir or else the inner boundaries move rapidly compared to stellar time scales.
3. Icy grains could persist for the lifetimes of the stars throughout the α PsA system and in the outer regions of the α Lyr and β Pic systems.
4. The ice sublimation time is only a few hours in the inner zone of the β Pic disk, so the grains there must be refractory, apparently confirmed by the detection of silicate emission close to the star (Telesco and Knacke 1991).
5. The maximum temperatures in the three systems are so different in terms of implied ice lifetimes that it seems unlikely the inner boundaries are all defined by a phase transition from icy to refractory grains unless the grain composition differs significantly from system to system.
6. Within uncertainties of grain density and radial structure the PR process is competitive with the collision process throughout these systems, although collisions appear to be generally dominant. If PR drag were in fact dominant, the existence of inner voids would require some additional mechanism to prevent grains from moving toward the stars and erasing the voids.

The time scales in Table XI clearly indicate that most of the small grains detected by IRAS are short-lived and must be replenished somehow. Detection statistics for analogs to the prototypes show that these systems are too common to represent chance detection of events as brief as the grain lifetimes.

Collisions can be a mechanism for production as well as destruction of small grains via destruction of larger bodies. Collisional or thermal fragmentation of undetected parent bodies to balance loss of the detectable grains were originally discussed by Weissman (1984), Harper et al. (1984), and Matese et al. (1987).

The grain lifetimes do not seem to offer a general explanation for the

inner boundary locations, temperatures, and surface densities of the three prototypes. It is possible that the inner boundaries reflect original structural features such as orbits of major planets. Planets orbiting the stars at the inner boundaries of the infrared-emitting regions and consuming or perturbing grains inbound under the influence of the PR effect could explain the central voids. On the other hand, in analogy with our solar system a large planet might result in an asteroid belt interior to its orbit which would be a source of extra dust, especially in a young planetary system. Surface photometry of the disks at $\lambda = 10$ to 20 μm with spatial resolution of 1 arcsec or better would be extremely valuable in constraining the sizes of the central voids and determining which processes are responsible for their creation and maintenance.

Minimum mass loss rates from collisions alone can be estimated by integrating Eq. (15) over radii, assuming that all the surface area is in grains with sizes as in Table III and density 1 g cm^{-3}. If this rate were to remain constant over the main sequence lifetime of the stars, a mass in small grains of at least 1×10^{-2} $M_\oplus$ for α Lyr and 1×10^{1} $M_\oplus$ for β Pic would be destroyed.

C. Speculation on History and Evolution

1. Protostellar and Protoplanetary Stages. The broad context of the study of protostellar and protoplanetary evolution tends towards elaboration of a basic planetesimal theory. This proceeds from the gravitational collapse of a rotating molecular cloud core to the formation of an optically thick circumstellar gas and dust accretion disk, which could be the precursor to optically thin grain disks like the ones under consideration here.

The choice between minimum-mass (see, e.g., Cassen and Summers 1983) and massive (see, e.g., Lin and Pringle 1990) protoplanetary disk scenarios is presently a basic controversy in the field of planetary formation. The relevance to this review is the question of origin of material at radii of 10^3 AU like the grains in the disk around β Pic, and by inference the other main-sequence far-infrared excess stars. In the minimum-mass scenario, material could reach that position via (1) the process of angular momentum distribution which dumps much of the initial disk into the star but greatly expands the scale of the remainder, and/or (2) orbital perturbation from the inner solar system; for example, many Uranus-Neptune zone planetesimals could be tossed outward by encounters with the nearly completed planets and found at intermediate semimajor axes of 10^2–10^3 AU, falling short of the Oort cloud. In contrast, in the massive-disk scenario planetesimals can form *in situ* at radii of 10^3 AU.

Calculations (Lin and Pringle 1990) of the evolution of massive disks show that the operation of some viscosity mechanisms makes any original surface distribution produced by infall eventually approach $\sigma_m(r) \propto r^{-1.5}$. This may indicate that the β Pic optical disk with $\sigma \propto r^{-1.7}$ from 100 AU to 1000 AU is a fossil remnant of an original disk rather than material sorted into that region by planetary perturbations.

At later development stages there is ample observational evidence that a

significant fraction of young main-sequence stars are surrounded by optically thick circumstellar disks of solar-system size with masses ~0.01 $M_\odot$ (Strom et al. 1989*d*; Beckwith et al. 1990) which corresponds to the entire disk in a low-mass scenario or the central portions of a more massive disk. Recent near- and mid-infrared (Skrutskie et al. 1990) and mm-continuum (Beckwith et al. 1990) studies of a large sample of pre-main-sequence stars in the Taurus-Auriga complex suggest that half of the known very young ($t<3$ Myr) solar-type stars have excess emission arising from heated dust embedded within such optically thick disks (see also Walter et al. 1988). At ages $t\geq 10$ Myr, fewer than 10% of the Taurus-Auriga sample show the infrared signatures of optically thick disks. Hence, disks apparently evolve from optically thick to optically thin structures. If all solar-type pre-main-sequence stars are initially surrounded by disks, then roughly half have either fully accreted their initial disk material or have begun to assemble grains into planetesimals by an age of 3 Myr and few optically thick disks survive for more than 10 Myr.

In a series of papers Nakano (1987*a*, *b*,1988) has attempted to extend a detailed theory of planetesimal and planet formation to explain the observations of β Pic and α Lyr in a self-contained way. This ambitious model is at odds in some ways with other planetesimal scenarios for the formation of our planetary system in having low initial disk mass and long time scales. Nakano (1987*a*) "finishes" Neptune in 3 Gyr, more than 1/2 the age of our solar system, whereas models of "runaway" accretion which begin with disks an order of magnitude more massive than the minimum mass produce planets much faster (Lissauer 1987) and put leftover material into substantial inner and outer Oort clouds. The most troubling disagreement between Nakano's model and observations of β Pic is that the model implies that we are viewing the star nearly in the disk midplane through significant optical depth ($\tau\sim 0.5$), but as discussed in Sec. V.A, the metallicity of β Pic explains the star's apparent low luminosity without extinction. Despite this and other problems, the value of these papers lies in the profound importance of the general issues raised by connecting the β Pic and α Lyr systems with theories of planet formation.

Nakano (1988) models the scattered light from the β Pic disk as due to small grains released by planetesimal collisions. He predicts an edge-on surface brightness of the disk following $r^{-4.375}$, quite close to the observed value $r^{-4.3}$, and also an approximately constant disk opening angle in the outer parts of the disk, agreeing with analyses of coronagraph observations. Nakano's model in addition predicts that there should be three regions in the β Pic disk, $r<4.7$ AU in which the planets are finished, $4.7<r<23$ AU in which the planetesimals have had at least one encounter and an equilibrium thickness has been reached, and 23 AU$<r<\infty$, a realm of colliding ice planetesimals which corresponds to the region visible in coronagraph images. The innermost region in the model represents a striking theoretical prediction of a central zone of the appropriate size which might be empty of small grains to the IRAS sensitivity limit. It is interesting that the outer region would not

be full of small grains but instead because of low planetesimal collision rates would contain discontinuous regions of relatively high density resulting from individual recent collisions, analogous to the asteroidal dust bands discovered in our solar system in IRAS data (Low et al. 1984; Sykes and Greenberg 1986). If this is true the surface brightness of a face-on disk would not be uniform but instead would be composed of myriad discrete and incomplete bands and streaks.

Planetesimal models of planet formation in general predict a progression of the planet formation process with time to greater radii, reducing the number of planetesimals and therefore the infrared luminosity from small grains. There would also be a decrease in the color temperature of the emission as the boundary between regions containing finished planets (no planetesimals) and unfinished planets (plus planetesimals and plentiful small grains) moves to greater radii. Nakano's models imply that a disk originally of β Pic's particle density and fractional luminosity would be more than an order of magnitude less prominent by an age of 5 Gyr.

2. *Encounters with the Interstellar Medium.* Lissauer and Griffith (1989) pointed out that erosion by dust grains in the ISM could be a significant destruction process for small grains orbiting far from a star like β Pic. This is true only if ISM grains can reach the circumstellar grains in the face of repulsion by the stellar luminosity; the work of Burns et al. (1979) and Artymowicz (1988) imply that very small grains may be relatively unaffected by radiation forces. The steady erosion of grains around stars with lifetimes of several times 10^8 yr or more would be mostly due to encounters with ISM grains in atomic clouds. The fragments would likely leave the circumstellar disk due to ISM gas drag, or radiation pressure, or ejection velocity above escape velocity.

Over a 100 Myr period in which no molecular clouds are encountered, erosion during the nominal 3% of the time spent in atomic clouds with $n_H \sim 20$ cm^{-3} would decrease a grain's radius by an average of $\Delta a = 50$ (v/10 km s^{-1})^3 μm. Note the dependence on v^3; that plus the fact that stellar random velocities are larger than cloud random velocities means that case-by-case stellar velocity will be important. The main point of the Lissauer and Griffith paper is that β Pic has a surprisingly low velocity relative to the "local standard of rest" (LSR), defined as the galactic circular orbital velocity vector for the solar neighborhood. The average motion of interstellar Ca II is within 3 km s^{-1} of the LSR (Mihalas and Binney 1981), indicating the LSR is a reasonable choice for the velocity frame of atomic clouds.

Lissauer and Griffith's conclusion is that β Pic's grains should be suffering markedly less ISM erosion than grains around other stars. This may provide an explanation as to why β Pic's disk density is so high and also why the typical grain size is so small compared to other examples. As further evidence, they find a weak correlation between grain luminosity $L_g/L_\star$ and stellar velocity for 10 nearby stars which have Vega/β Pic analog far-infrared excesses.

Whitmire et al. (1992) propose instead that passage through a dense re-

gion of the ISM would act to temporarily *increase* the total grain area around stars via multiple-impact fragmentation of large grains in pre-existing disks. The grains in our inner solar system which have been produced by asteroid collisions or released from active comets have typical sizes of 100 μm (Grün et al. 1985). This is roughly the same size as the grains in the α Lyr disk. Whitmire et al. argue that multiple collisions during passage through an atomic cloud could result in destructive fragmentation even of large grains. In this scenario most circumstellar disks are in quiescent states of low detectability during which large grains are produced by parent body collisions or sputtering. This alternates with brief periods during which the large grains suffer fragmentation so that detectability is greatly enhanced until the various internal removal mechanisms clear out the small grains.

Whitmire et al. (1992) show that five A stars with the most luminous circumstellar disks or candidate disks (α Lyr, α PsA, β Pic, β Leo and ζ Lep) have space motions which are highly correlated. The trajectories of all 5 of these stars passed through or near the Lupus-Centaurus (also called Sco-Cen) ISM concentration (d = 100–200 pc) between 5 and 10 Myr ago. Although groups of stars with small dispersion velocities in at least two components are usually young stars of common origin which can often be associated with a known concentration, this is unlikely to be the explanation for this group of 5 stars because their mean velocity is not close to that of objects in the Lupus-Cen concentration or any other known concentrations. Also, evidence in Sec. V.A indicates that the ages at least of α Lyr and β Pic are discordant, and both stars are much too old to have formed in Lupus-Cen. Another explanation would be a selection effect whereby stars which independently passed through the nearest concentrations of the ISM call attention to themselves by their newly enhanced small-grain far-infrared excesses. Such stars which are currently in our vicinity would necessarily have similar velocity vectors.

The essential differences between the Lissauer and Griffith and the Whitmire et al. scenarios is that the former group imagines an initial population of grains of a range of sizes down to 1 μm which is not replenished but is eroded progressively except in special cases of low stellar velocity. The latter group imagines continual replacement of large grains which are episodically converted into smaller grains.

3. Post-Main-Sequence Evolution. Matese et al. (1989) investigated the question of the fate of circumstellar disk material when the parent star leaves the main sequence and progresses through red giant and asymptotic giant branch (AGB) stages. The luminosity of 1 to 2 $M_\odot$ stars increase by factors of 10^3–10^4 during these stages over periods of 10^7–10^8 yr, with corresponding increases of circumstellar grain temperatures by factors up to 10. For example, small water ice grains located anywhere within 10^4 AU of β Pic would be heated to above sublimation temperature and be rapidly destroyed. Larger icy parent bodies would become active and release gas and grains as comets do in our inner solar system.

Matese et al. conclude that the grain release rate from activated comets is

probably not sufficient to supply the grain mass observed in AGB star winds usually interpreted as condensing directly from the wind material. However, small grains from the comets could provide the necessary cores on which the AGB stellar mass loss would condense into larger grains. The source of those nucleation cores has been somewhat of a puzzle in ISM grain and AGB star research especially given the fact that other types of stars (e.g., hot supergiants and most Wolf-Rayet stars) have significant mass loss but negligible grain condensation. Their model of the environment of AGB stars yields testable predictions of grain condensation location and morphology of the grain flow (flat rather than spherical) which differ significantly from the predictions of classical nucleation theory. Jura (1990) (see also Judge et al. 1987) finds that less than 5% of G–K *giants* have far-infrared excesses in IRAS PSC data. G giants are mostly descendants of A–F main-sequence stars, do not generally show signs of mass loss, and precede the AGB evolutionary stage. If giants had disks with optical depths like those seen around at least 20% of nearby main-sequence stars, they would have had detectable excesses (a G giant has about 3 times the luminosity of its A main-sequence progenitor). Jura concluded that either main-sequence circumstellar grains are destroyed by PR drag without resupply, or the grains are icy such that grains originally near 100 K are quickly destroyed by small temperature increases at the beginning of post-main-sequence evolution.

VI. RELATIONSHIP TO OUR SOLAR SYSTEM

The crucial question of the relation of these Vega/β Pic systems to our solar system and to planetary systems in general needs to be addressed. If the examples of cool debris around main-sequence stars detailed in Sec. IV are each sign of a planetary system, then the Drake equation factor expressing the fraction of stars with planets f_p can be estimated to be greater than 0.15 based on these IRAS investigations.

A. Planetary Systems Around The "Big 3" Prototypes?

As previously discussed, there is evidence that the infrared radiating material in all three prototypes probably lies in a disk in the stellar equatorial planes. Central clearings of solar system scale have been found in these examples because flux densities are high enough to allow a plausible determination at IRAS sensitivity of a maximum grain temperature. This has been interpreted as evidence that planets have accreted and removed an original small grain population from detectability (Diner and Appleby 1986). On the other hand, the depleted zones could also be regions cleared of ice grains by sublimation, or could signify a failure of any material to accumulate in those areas when these systems formed.

Weissman (1984) and Harper et al. (1984) have suggested that the emission around α Lyr is from small grains generated by sublimation or collisions in a cloud of comet-like bodies similar to that thought to have condensed in

the outer solar system. Weissman pointed out that it was improbable that planetary-sized bodies are present in the far-infrared emitting region itself because the accretion time for large bodies at these distances from the star are longer than the age of the system.

In the β Pic system, there may be a planet-mass perturber propelling dust particles close to the star to produce the transient absorption line events (Beust et al. 1991). The grain evaporation products may accumulate in a coma of ions observed in the stable heliocentric component of the Ca ion representing the massive "classical" shell.

B. Infrared Detectability of Our Solar System from "Outside"

One can consider how our solar system would appear to an instrument with IRAS' capabilities if viewed from β Pic ($d \sim 16$ pc).

1. The Sun itself would be detectable only at 12 and 25 μm. The diameter of the planetary region (Pluto's orbit) would subtend 5 arcsec. The sum of the infrared flux from the planets, moons, and large asteroids would be a factor of 10^4 below IRAS' best sensitivity limit in "pointed" observations.

2. The bolometric luminosity of the zodiacal dust in the inner solar system is about 8×10^{-8} $L_\odot$, with characteristic temperature of 230 K and typical grain sizes of 100 μm (Good et al. 1986; Grün et al. 1985) The presence of that material would produce at $\lambda \sim 20\,\mu$m (best contrast) a tiny excess of 2×10^{-4} Jy, less than 10^{-2} of IRAS' limit, on top of a solar photospheric flux density of 0.2 Jy. The emission would be contained within a diameter of less than an arcsec. Not only would the signal be too small in an absolute sense, but without high spatial resolution even a sufficiently sensitive infrared instrument would need to be coupled with extremely precise knowledge of the Sun's photospheric infrared spectrum to identify that amount of nonphotospheric emission.

This illustrates once again the principle that direct detection of optical or infrared radiation from extra-solar planetary material is sensitive to area rather than mass; the zodiacal dust contains less than 10^{-10} of the total mass of the planets, yet has an infrared luminosity 10^2 times larger. It is possible that other planetary systems might have more prominent zodiacal clouds. A zodiacal cloud around α Centauri with roughly twice the particle area of our own would be barely within the best sensitivity limit of IRAS in an ideal sense, but that star is seen against the background of a dense stretch of the galactic plane which frustrates attempts at sensitive searches.

3. The classical Oort cloud from which long-period comets are believed to come (see, e.g., review by Weissman 1990), contains of order 100 $M_\oplus$ in comet nuclei (typical radii of order 10 km). These bodies orbit at least 2×10^4 AU (0.1 pc) from the Sun out to an outer limit of roughly 1.5×10^5 AU (0.75 pc) set by encounters with other stars and the galactic tide (Heisler and Tremaine 1986). Objects in this range of radii are loosely enough bound to the Sun that encounters with passing stars can perturb them into orbits that pass into the planetary region. Our Oort cloud would subtend a diameter of 5°

when viewed from β Pictoris. This would allow easy spatial resolution, but the material would be undetectable to IRAS if the mass were contained solely in comet-sized bodies because the total surface area and thus the luminosity would be extremely small (Stern 1990). Also, the temperature would be less than 5 K and its emission would be difficult to find in contrast with galactic material and cosmological background radiation. Therefore, if the classical Oort cloud consists only of larger bodies, it would not be seen by IRAS from a distance of 16 pc. Stern (1990) noted that erosion by ISM grains should result in the production of small grains and greatly enhanced surface area and detectability, but a search of several nearby stars resulted in no detections and an appreciation for how dirty the Galaxy is at the relevant wavelengths.

4. Many authors have speculated that the process of forming the Oort cloud could have left as much as 5 to 100 times more mass in a so-called "inner Oort cloud" or "Hills cloud" than in the classical Oort cloud (see, e.g., Tremaine 1990; Weissman 1990). If there are in fact objects closer to the Sun than about 2×10^4 AU, their orbits are more tightly bound than orbits in the classical Oort cloud and thus are not usually perturbed into the planetary region. The inner Oort cloud is imagined as a plausible central concentration of the known Oort cloud which might approximate a disk in its inner regions ($r \leq 5000$ AU; Tremaine 1990) but would tend towards sphericity in transition to the outer observed Oort cloud due to perturbations from passing stars.

Note that the "maximum" mass estimates for the resolved circumstellar disks in Table III are in the same range as estimates of the mass of the inner Oort cloud, which more than doubles the minimum gas mass needed in the original protoplanetary disk. However, even this large amount of material would have too little surface area for the IRAS sensitivity limits if it consisted only of large bodies. Also, material at $r > 100$ AU around the Sun would be colder than 30 K which is the approximate limiting temperature for good contrast to background material at low galactic latitudes. From β Pic the Sun appears near the boundary between Draco and Hercules, at $b_{II} \sim 30°$, so the limiting temperature in this specific hypothetical case might be cooler.

In summary, given the known characteristics of our system, IRAS would detect nothing from $d = 16$ pc at temperatures corresponding to the planetary region, $T > 50$ K, $R < 30$ AU, and the amount of material known or hypothesized to exist at $T < 30$ K, $R > 100$ AU is insufficient for IRAS sensitivity. The region of potential IRAS detection by process of elimination is therefore the region roughly between 30 and 100 AU from the Sun lying just outside the planetary region which may contain the Kuiper belt.

C. The Kuiper Belt

The Kuiper belt is imagined alternatively as (1) an extension of the protoplanetary disk in which low density of planetesimals and long encounter time scales prevented the formation of planets, or (2) a region into which Uranus-Neptune planetesimals were propelled during the formation of those planets. An excellent review of limits on "dark" (undiscovered) matter in the solar

system, including speculation regarding the properties of the Kuiper belt, has been written by Tremaine (1990). The simplest reason to believe there may be such a structure is the low inclination to the ecliptic of the orbits of short period ($P < 20$ yr) comets, also known as "Jupiter-family" comets. There is no simple way to produce this population dynamically unless their reservoir is a flattened system, in contrast to the Oort cloud (long-period) comets which have random inclinations and thus probably a spherical reservoir. Figure 9 shows that the surface density of the planetary region follows a power law which when extrapolated predicts about 5 $M_\oplus$ in the region between 30 and 100 AU, below the present limits of detectability placed by measurement of planetary and spacecraft motions.

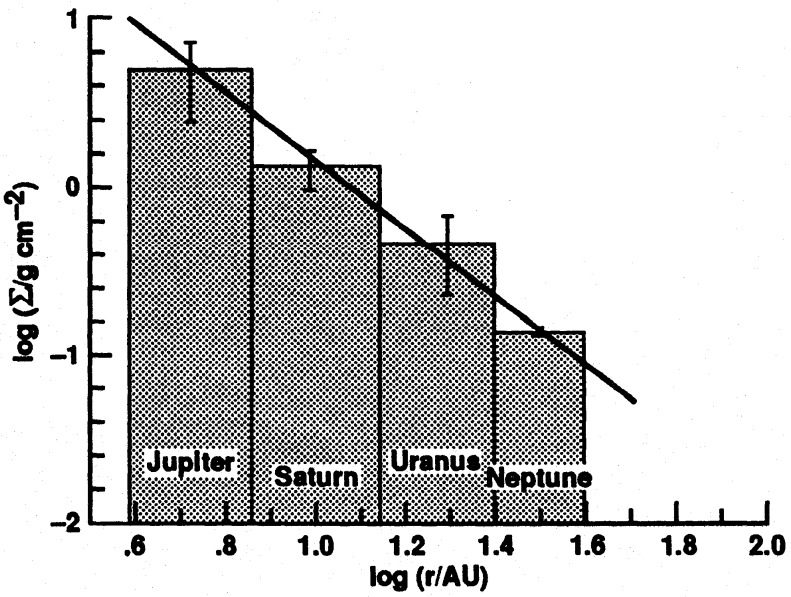

Figure 9. Mass surface density profile of the solar system if each Jovian planet's mass were spread half-way (in a logarithmic sense) to the adjacent planets. This can be imagined to represent the pre-solar nebula's surface density at some stage during the formation of the solar system. It is possible that the mass distribution continues beyond the known planets, allowing roughly 1 to 10 Earth masses to reside between 30 and 100 AU from the Sun in some form.

If one imagined that the nearby stars all have planets, zodiacal clouds, Kuiper belts, and Oort clouds with approximately the characteristics of the components of our planetary system, an instrument like IRAS would be sensitive only to the Kuiper belt component temperatures and scales. Table XII summarizes the detectability of the components of our solar system and makes comparison to the general properties of the Vega/β Pic systems. The radius in this table characterizing the main-sequence grain disks is not the outer radius, but rather is the far-infrared size of the three resolved systems and the peak surface density in models of the β Pic disk. The best analog in scale to the

main sequence disks is the Kuiper belt. However, if only large bodies (comet nuclei) exist there, the solid surface area is insufficient for infrared detection.

TABLE XII

Circumstellar Dust Properties

Location	R (AU)	T (K)	Log Area, AU^2	Log $L_g/L_\star$	Morphology
Zodiacal Dust	3	200	−5	−7	flattened
Kuiper Belt (1 $M_\oplus$,10 km objects)	> 50	40	−5	−9	flattened
Kuiper Belt (1 $M_\oplus$, 10 μm–10 km size distr.)	> 50	40	0	−5	flattened
Typical M.S. Grain Envelopes	100	30–150	0–2	−5 to −3	flattened ?
Oort Cloud (100 $M_\oplus$, 10 km objects)	10^4	3	−5	−12	spherical

An order-of-magnitude check on the plausibility of our solar system having a collection of small grain fragments from Kuiper-belt comet collisions shows that such a disk would have a grain area very comparable to Vega/β Pic disks. If 1 $M_\oplus$ of 10 km bodies with material density 1 g cm^{-3} are imagined confined between 30 and 100 AU from the Sun (figure from Tremaine 1990), the collision time per parent body is about 10^{11} yr so that most of them would be intact at the present age of the solar system. The number of collisions per year throughout the region would be approximately 10^{-1}.

If the fragments from each collision are assumed to have an $a^{-3.5}$ size distribution running from a minimum size somewhere in the range of 1 to 100 μm (like dust in comet comae, the zodiacal cloud, and the prototype main-sequence far-infrared sources) to a maximum size of 1 km (1/10 the size of the parents), then the PR destruction time scale for the smallest grains (those dominating the surface area and therefore the most detectable) would be in the range 10^6 to 10^9 yr depending on original orbit radius. The total amount of new small grain fragments produced by parent collisions during a PR time scale would yield a small-grain optical depth perpendicular to the ecliptic plane at r = 30–100 AU in the range 1 Myr to 1 Gyr strikingly similar to the lower range of extrasolar examples. The small-grain mutual collision time scale in this case would be less than but within an order of magnitude of the PR time scale, just like in the 3 prototype sources. In the case of our Sun, the distances would make the characteristic temperature of the emission 50 K or colder.

D. Steps Toward a Connection

Is it true, then, that what we are observing with IRAS around nearby main-

sequence stars corresponds to their "Kuiper belts"? There are at least three ways to investigate the connection. *First,* are there planetary perturbations in any of the IRAS-detected systems, and where do the massive objects lie with respect to the IRAS material? *Second,* can systems be found with material at warm temperatures/radii corresponding to the planetary zone along with cooler Vega-type material? In other words, are the phenomena of clear zones in the "Big 3" resolved systems, and also the general lack of detection of material warmer than roughly 200 K around nearby stars (Aumann and Probst 1991), signs of *failed* planetary systems or *completed* planetary systems? *Third,* does our solar system have a cool grain disk outside the planetary zone?

1. Solar-Type Stars With Planetary Perturbations. Campbell et al. (1988*b*) investigated 12 slowly rotating, single, bright F-K dwarfs for radial velocity variations in the first search sensitive enough to find Jupiter-mass planets. Their technique depends on passing starlight through a cell of hydrogen fluoride which provides sharp-reference velocity lines insensitive to effects like flexure in the spectrograph. Their resulting mean external error is about 13 m s^{-1}.

Seven stars in the sample have marginal detections of velocity trends over 8 years' time, some with concavity or convexity implying periods of order a decade, although no system has been seen to go through a full cycle yet. There is no correlation between the radial velocity variations and stellar activity indicators such as equivalent line widths of Ca II H and K line emission. If the perturbations are real, the implied sizes of the companions are of order 1 to 10 Jupiter masses.

The significance of these results in the context of this review is that one of the systems with possible Jovian companions, ϵ Eri, is an IRAS far-infrared excess system. The emission temperature of 70 K could indicate material within or beyond the region of planetary companions, depending on grain size. The other six Campbell candidates do not have far-infrared excesses at IRAS sensitivity and thus would be prime targets for observation with more sensitive future instruments such as ISO or SIRTF.

2. Young Stars with Hot Debris. Calculations of collision dynamics and orbit evolution of planetesimals in our solar system yield a particle number density 1000 times larger than the present value as late as 500 Myr after the Sun reached the main sequence, with about a 100 Myr half-life for subsequent decline (Grinspoon 1988; Grinspoon and Sagan 1991). Witteborn et al. (1982) calculated the amount of infrared radiation which would be emitted from an $a^{-3.5}$ size distribution of grains and planetesimals orbiting main sequence stars assuming a spatial distribution like that of the planetary masses in our solar system. Their results are that 80% of the infrared excess will come from warm material in the "terrestrial" region despite the 100 times larger mass in the Jovian region, and that 1% of the solid mass of the planets is easily found at 10 to 20 μm if the photosphere of the parent star is detectable. This mass corresponds to the particle number density calculated for roughly 200 to

500 Myr after the formation of the solar system. Backman et al. (1990) made a study of coadded IRAS survey data on main-sequence A stars in open clusters younger than 1 Gyr. IRAS photometry was not accurate enough to discern individual stars in most cases because of the distances to the clusters, but statistical statements can be made about the presence or absence of infrared excesses in the cluster stars considered as groups. There appears to be greater emission from A stars at 12 μm in the younger two clusters than in the older two. The trend with age may represent progressive destruction or accretion of grains.

Although the Pleiades are passing through a molecular cloud that is responsible for the spectacular optical reflection nebulae (Breger 1987), and calculations of radiation pressure efficiency imply that very small grains like ISM grains might be able to come close to luminous stars, the 12 to 25 μm ratios suggest that ambient cloud grains are not the cause of the observed excesses. Assuming that a thin undisturbed distribution of grains around an unrelated star would be roughly $n(r) \sim r^0$, the expected thermal emission spectrum from ISM-size grains would rise steeply toward longer wavelengths, $F_v \sim \lambda^2$, because of the increase of grain number with distance (cf. Eq. 10).

These results need to be confirmed via groundbased observations especially in light of Aumann and Probst's (1991) studies of false 12 μm excesses around nearby field stars. Also, sub-millimeter searches for this effect in the same clusters have returned null results (Zuckerman, personal cummunication) although that technique would be somewhat less sensitive to material at warm temperatures. Unfortunately these clusters are so distant that IRAS data could not be used to check for complementary cool excesses with properties like the Vega/β Pic systems, so a direct comparison of location of material around the cluster stars versus generally older nearby field stars will have to await future instruments such as ISO or SIRTF.

3. Does Our Solar System Have a Cool Grain Disk? If our solar system had a grain disk outside the planetary region in the region corresponding to the Kuiper belt, it is surprising but true that grain surface area and temperatures like the examples turned up in IRAS surveys would be difficult to detect from *inside* because of the powerful interference viewed from Earth of bright warm foreground zodiacal dust. Backman and Gillett (1987) and Aumann and Good (1990) found that the difference between IRAS scans at 60 and 100 μm of the zodiacal dust emission in the ecliptic plane, and models of the expected emission, could represent some emission from material beyond the planetary region. It is possible that all the emission observed is actually in the inner solar system and will be explained in the future by more sophisticated models of the zodiacal cloud. However, the uncertainties at this point in our knowledge of the zodiacal system *allow* a disk at temperatures below 40 K, located at $r > 50$ AU, with total optical depth somewhat smaller than the material around α Lyr.

The upper limit on optical depth for such a cloud is larger than the apparent mean amount of material observed in ensemble for nearby G dwarfs.

Aumann and Good (1990) argue that, since the typical G dwarf appears to have some cool circumstellar material, it would be peculiar if the Sun *did not*. If there is such material in our solar system, it cannot be concentrated too strongly towards the ecliptic plane, or its surface brightness would be too large. "Wedge" angles ι greater than 5° are consistent with the observations.

Tremaine (1990) points out that upper limits on number density of comet-nuclei-sized bodies in the Kuiper belt from the best present optical searches are just beginning to approach values corresponding to upper mass limits from dynamical calculations. Cruikshank et al. (1990), however, find that these bodies might be detectable with SIRTF.

VII. SUMMARY AND FUTURE DIRECTIONS

A detailed understanding of the genesis of planets is one of the major goals for the astronomical community, equal in import to investigation of the origin of the universe as a whole. The IRAS mission resulted in the startling discovery that normal main-sequence stars often host cool orbiting grains with likely but not certain connection to planets. The state of our knowledge about these systems after the IRAS mission can be divided into three categories: (a) a few systems close enough/luminous enough that hints of shape and structure have been discerned; (b) one hundred or more stars with cool far-infrared excesses but without IRAS spatial resolution or sufficiently good photometry to demonstrate conclusively that the emission is due to orbiting grains rather than to possible alternate mechanisms; and (c) most stars, up to 80% of the nearby A-K dwarfs and all but one M dwarf, with no circumstellar material apparent at IRAS sensitivity.

Future infrared observations should aim to: (1) explore the three prototype disks in detail, addressing questions of radial and azimuthal symmetry and precise nature of boundaries; also, perform reflectance mineralogic spectroscopy where possible; (2) spatially resolve IRAS candidates, checking whether the sources are centered on the stars (i.e., not background) and are disks in the stellar equatorial planes, estimating grain sizes from angular scale vs temperature, and performing sufficiently precise photometry that maximum temperatures (inner boundary locations) can be deduced; and (3) search for grains around stars with IRAS nondetections; a hundred-fold better sensitivity would make detection of systems as sparse as our solar system's zodiacal dust cloud possible in some circumstances.

The story behind the origin, maintenance and destruction of such disks will gradually become clearer as main-sequence circumstellar disks come to be understood in the context of stellar evolution. For example, we can ask what type of circumstellar disks normally remain after star formation? This could be answered by further examination of classical and "naked" (weak) T Tauri stars and open cluster stars, with ages of order 10^7 to 10^8 yr, in order to investigate inner disk clearing time scales and persistence of outer disks. Also, what happens to these disks when the stars evolve off the main

sequence? This calls for further observations of evolved stars in search of evidence of increased sublimation and possible augmented dust nucleation occurring when remnant disks are exposed to post-main-sequence luminosity increases and mass loss. Finally, do such disks represent success or failure modes in planet building? We need to continue searches of the distant regions of our own solar system's ecliptic plane for evidence of planetesimal-sized parent bodies and collision fragments, and to compare expanded lists of infrared excess stars with lists of suspected planetary-mass astrometric and spectroscopic binary companions. We can hope for eventual firm knowledge of the frequency with which normal stars possess material left over from the process of planet formation.

Acknowledgment. D. B. acknowledges a National Research Council post-doctoral fellowship, a NASA Origins Initiative grant, the NASA-Ames SETI Institute, and Franklin and Marshall College for support. We thank F. Witteborn, M. Werner, P. Cassen, J. Lissauer, P. Artymowicz, and the referee M. Skrutskie for many helpful comments. We also thank A. Graps for computer searches relating to stellar surveys and N. Jennerjohn for assistance in preparing the tables and references.